Tectonics®

RESEARCH ARTICLE
10.1029/2025TC009045

Rapid Transition From High-Pressure Metamorphism to Exhumation Driven by Orogen-Parallel Extensional Shearing (Adula Unit, Eastern Central Alps)

C. Montemagni[1], R. Monti[2], N. Malaspina[2], P. Vannucchi[1], and S. Zanchetta[2]

[1]Department of Earth Sciences, University of Florence, Firenze, Italy, [2]Department of Earth and Environmental Sciences, University of Milano Bicocca, Milano, Italy

Key Points:

- First dated Alpine eclogites in the northern Adula unit by means of $^{40}Ar/^{39}Ar$ geochronology extend Alpine high-pressure (HP) metamorphism northward
- Peak Alpine HP metamorphism, 2.0–2.4 GPa and 580°–655°C, recorded at a minimum age of 38–39 Ma
- Switch from nappe stacking to extensional shearing within ∼5 Myrs

Supporting Information:

Supporting Information may be found in the online version of this article.

Correspondence to:

C. Montemagni,
chiara.montemagni@unifi.it

Citation:

Montemagni, C., Monti, R., Malaspina, N., Vannucchi, P., & Zanchetta, S. (2026). Rapid transition from high-pressure metamorphism to exhumation driven by orogen-parallel extensional shearing (Adula unit, eastern Central Alps). *Tectonics*, *45*, e2025TC009045. https://doi.org/10.1029/2025TC009045

Received 11 JUN 2025
Accepted 4 FEB 2026

Author Contributions:

Conceptualization: C. Montemagni, S. Zanchetta
Data curation: C. Montemagni
Formal analysis: C. Montemagni, R. Monti, S. Zanchetta
Funding acquisition: S. Zanchetta
Investigation: C. Montemagni, R. Monti, N. Malaspina, S. Zanchetta
Methodology: C. Montemagni, N. Malaspina, S. Zanchetta
Project administration: S. Zanchetta
Supervision: C. Montemagni, S. Zanchetta
Validation: C. Montemagni, S. Zanchetta
Writing – original draft: C. Montemagni, S. Zanchetta

Abstract In the Central Alps, the Adula unit exposes high- and ultra-high-pressure (HP-UHP) metamorphic rocks, providing key insights into the subduction and exhumation dynamics of the former distal European margin. We investigate the San Bernardino Shear Zone (SBSZ), a top-to-the-east extensional shear zone developed within orthogneiss and paragneiss at the top of the Adula unit, containing eclogite boudins. Using detailed structural analysis, petrography, thermodynamic modeling, and $^{40}Ar/^{39}Ar$ geochronology, we constrain the Pressure-Temperature-deformation-time (*P-T-d-t*) path of these high-pressure (HP) rocks. Phengite in eclogites yields minimum age of peak metamorphism of 38–39 Ma, making them the northernmost Alpine HP record in the Adula unit. Eclogite facies conditions reached ∼2.0–2.35 GPa and 580°–655°C. Progressive deformation in the eclogite host rocks led to the overprinting of earlier NW-directed fabrics by top-to-the-east shearing, recorded in synkinematic mica and associated with resetting of $^{40}Ar/^{39}Ar$ ages to 36–29 Ma. This temporal-spatial pattern indicates a short interval between subduction, nappe stacking, and extensional exhumation. Our results demonstrate that the SBSZ played a key role in the exhumation of the eastern Lepontine Dome, supporting a model of distributed orogen-parallel extension. This mechanism, partially coeval with amphibolite-facies metamorphism and crustal anatexis, suggests that HP units were exhumed during orogen-perpendicular shortening and orogen-parallel extension.

1. Introduction

The exhumation of high-pressure (HP) and ultra-high-pressure (UHP) metamorphic rocks in collisional belts has been a central topic of tectonic research for decades, yet significant debate remains over the geometry and driving mechanisms behind these processes (see Hacker & Gerya, 2013 for further discussion). One ongoing issue is the extent of tectonic re-organization observed in HP units. Some works (e.g., Engi et al., 2001; Trommsdorff, 1990) argue that what appear to be coherent HP units are actually tectonic mélanges, where units of various origin and nature have been mixed along the plate interface (TAC: Tectonic Accretion Channel; Engi et al., 2001) during the subduction–exhumation cycle. These units, with their distinct Pressure-Temperature-deformation-time (*P-T-d-t*) paths, possibly recording multiple cycles of subduction and exhumation over a few million years (e.g., Gerya et al., 2002; Rubatto et al., 2011), might have been assembled in what seems now a coherent tectonometamorphic unit.

Chaotic mixing models have become increasingly popular for oceanic HP units (e.g., Federico et al., 2007; Gerya et al., 2002; Vannucchi et al., 2012), which commonly contain serpentinite-dominated matrix incorporating fragments of continental and oceanic crust and mechanically weak structures. For continental HP units instead, the relevance of subduction-channel mélange models is more uncertain, with some Authors (e.g., Chemenda et al., 1995; Nagel, 2008) suggesting that entire coherent (U)HP units are exhumed during single events. Field, petrological and geochronological evidence, as well as numerical modeling, instead suggests that also thin continental crust units can be subducted and later exhumed diachronously along a subduction channel (e.g., Stöckhert & Gerya, 2005) in both ablative and non-ablative subduction settings (Regorda et al., 2021; Roda et al., 2012).

In these scenarios the syn convergence exhumation reflects the interplay between crustal thickening and extensional shearing that facilitates the return of deeply subducted material to the surface. Classical examples include the Himalaya (e.g., Grujic et al., 2011) and the Alps (e.g., Malusà et al., 2015), but similar processes have been documented, for example, in the Taiwan orogen (e.g., Beyssac et al., 2008).

Writing – review & editing:
C. Montemagni, R. Monti, N. Malaspina, P. Vannucchi, S. Zanchetta

The Adula unit in the Lepontine Dome of the eastern central Alps (Figure 1) is one of the classical areas of the Alps where (U)HP eclogite-facies metamorphism occurred (e.g., Nagel, 2008). This unit consists of various gneisses with calcschists, marbles and the local occurrences of eclogites and garnet peridotites in the Cima Lunga subunit (Heinrich, 1986).

The Adula unit was suggested to be a chaotic subduction channel mélange (Trommsdorff, 1990), with some studies concluding that it consists of rocks from different paleogeographic origins and/or distinct subduction histories (e.g., Berger et al., 2005; Engi et al., 2001; Trommsdorff, 1990), possibly already formed as a melange during the Variscan orogeny (Tagliaferri et al., 2023). Other researches, however, suggests it represents a relatively coherent basement unit, at least since peak-pressure conditions during the Alpine event (e.g., Cavargna-Sani et al., 2014; Dale & Holland, 2003; Herwartz et al., 2011; Nagel, 2008; Ring & Glodny, 2021).

In this context, it is critical to unravel the tectonometamorphic history of the whole unit, from HP conditions to nappe stacking within the Lepontine Dome and its final unroofing. Available data suggest the occurrence of a regional Barrovian overprint of the HP rocks occurred in a very short time span after the pressure peak (e.g., Piccoli et al., 2022; Tagliaferri et al., 2023; Tumiati et al., 2018). Such overprint occurs, with southward increasing peak temperatures (e.g., Burri et al., 2005), in the whole Lepontine Dome that represents a crustal nappe stack made of tectonic units derived from the distal margin of the European plate, the Mesozoic basins and the Briançonnais microcontinent (Handy et al., 2010; Stampfli et al., 1998). These units were stacked together northward (e.g., Nagel, 2008) and later up-arched to form the dome during the late Eocene-Oligocene continent-continent collision (e.g., Merle & Guillier, 1989; Schmid et al., 1996; Steck et al., 2013; Wiederkher et al., 2009). The up-doming of the Lepontine Dome was accommodated by several crustal-scale shear zones at its boundary. To the West, the extensional Simplon Fault (Figure 1a; e.g., Mancktelow, 1985) promoted the exhumation of the western part of the Dome (the Toce culmination) between 20 and 8 Ma (see Montemagni & Zanchetta, 2022; Wolff et al., 2024 for updated reviews). To the East (the Ticino culmination), no prominent structures such as the Simplon Fault occur, but a series of post metamorphic minor extensional faults (Figure 1a; Rahn, 2005; Tagliaferri et al., 2023) between the Europe-derived units or in the Austroalpine (i.e., Africa derived tectonic units) in the hanging-wall of the Dome (Ring & Glodny, 2021).

However, extensional shearing at the top of the eastern termination of the Lepontine Dome is not only confined in the hanging-wall Austroalpine units, but significant crustal extension has been likely accommodated also within the Adula unit. In the San Bernardino Pass area (Figure 1b) in South Switzerland we identified a shear zone (the San Bernardino Shear Zone (SBSZ) developed within orthogneiss and eclogite-bearing paragneiss layers at the top of the Adula unit. By means of detailed geological mapping, meso- and micro-structural analysis, petrography, geothermobarometry and $^{40}Ar/^{39}Ar$ dating, we reconstructed the *P-T-d-t* (Pressure-Temperature-deformation-time) paths of the eclogites and the hosting rocks. The San Bernardino eclogites, dated for the first time, resulted to be the northernmost HP rocks of Alpine age in the Adula unit. The occurrence of eclogites within the SBSZ allowed us to have a complete view from the Alpine HP stage to the exhumation of eclogites passing through the regional Barrovian overprint. The wealth of data helped to pinpoint the role of this extensional shear zone in the exhumation of the (U)HP Adula unit and the eastern part of the Lepontine Dome.

2. Geological Background

The Central Alps started to form in the middle Eocene in response of the closure of the Mesozoic Alpine Tethys and the collision between the southern European and northern Adriatic margins (e.g., Handy et al., 2010; Stampfli et al., 1998). The continent-continent collision took place in the late Eocene—early Oligocene following the subduction beneath northern Adria of the oceanic lithosphere and related sediments of the Alpine Tethys oceanic basin, as well as part of the European continental crust (Gebauer, 1996; Schmid et al., 1996; Wiederkehr et al., 2009).

As a consequence of collision, the European basement nappe were thrust northward between 33 and 36 Ma forming the Penninic nappe-stack of the Central Alps (Cavargna-Sani et al., 2014; Kossak-Glowczewski et al., 2017; Nagel, 2008; Nagel et al., 2002; Rahn, 2005; Steck et al., 2013; Wiederkehr et al., 2008, 2009). After or during nappe stacking (see Tagliaferri et al., 2023 for discussion) a Barrovian metamorphism affected all the Penninic tectono-metamorphic units forming the Lepontine Dome, with concentric isotherms that crosscut nappe boundaries (Figure 1b). Temperature increases southward, reaching a maximum within the Southern Steep Belt (Figure 1b), close to the Periadriatic Fault, where diffuse migmatisation occurred (e.g., Burri et al., 2005).

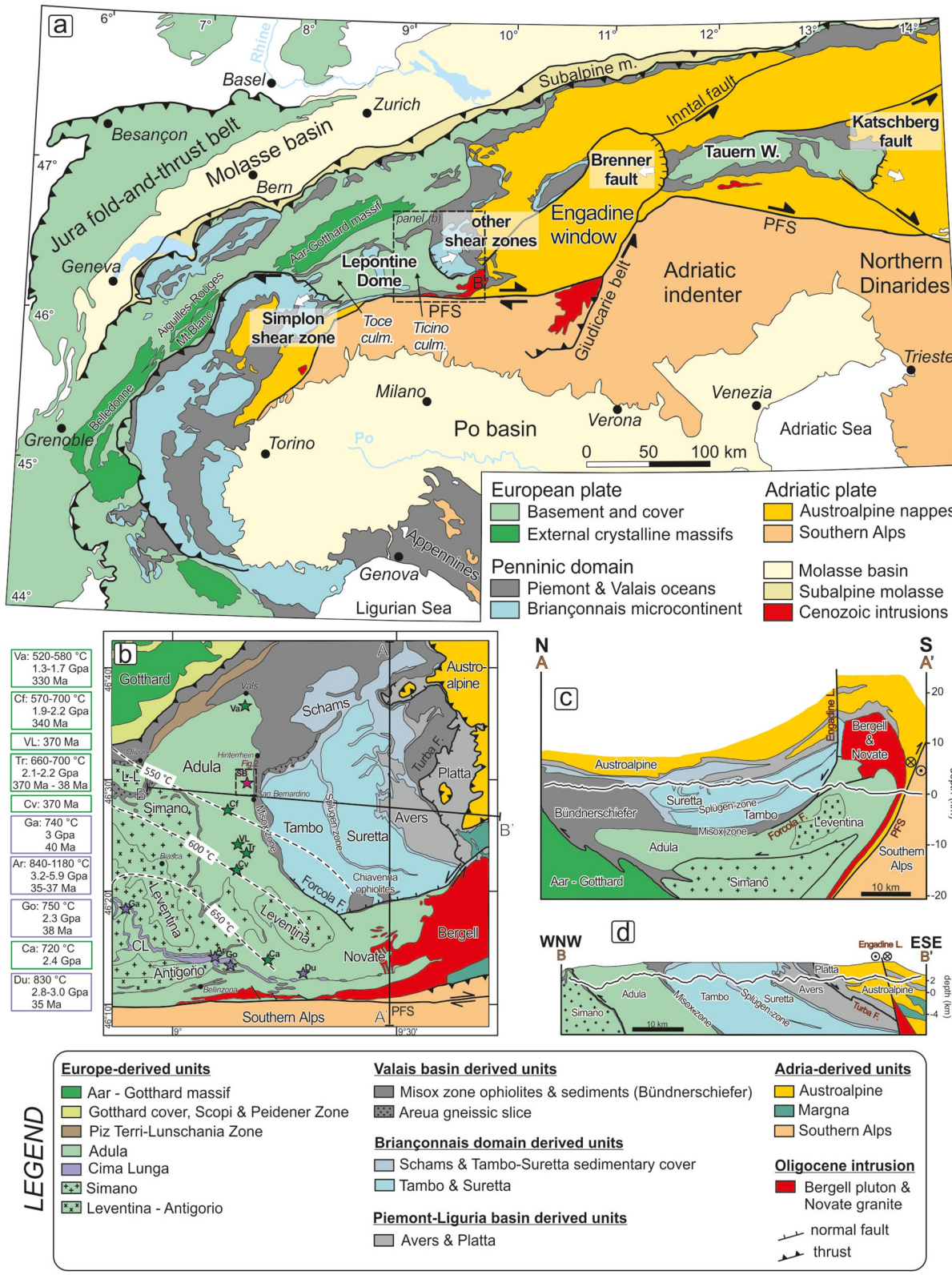

Figure 1.

The tectono-metamorphic units of the Lepontine Dome derive from the hyperextended European margin and from the Alpine Tethys and the Briançonnais microcontinent (Schmid et al., 2004) that separated the Alpine Tethys Ocean in two basins (N and S Penninic oceans, Handy et al., 2010). The several units experienced heterogeneous *P-T* paths before the nappe-stacking phase and the formation of the Lepontine Dome (e.g., Tagliaferri et al., 2023).

The Adula unit, together with Simano and Lucomagno-Leventina units, belongs to the Lower Penninic nappe complex derived from the distal European margin of the Helvetic domain. At present Adula unit lies below the Tambo and Suretta Middle Penninic nappes derived from the Briançonnais domain, which originally formed a horst structure between a marginal ocean basin (Valaisan trough) to the N and an open ocean to the S (Figure 1b; e.g., Cavargna-Sani et al., 2014; Gebauer, 1996; Nagel, 2008; Nagel et al., 2002; Pleuger et al., 2003; Schmid et al., 2004; Steck et al., 2013, 2019; Wiederkehr et al., 2009). According to paleogeographical reconstructions (Schmid et al., 2004), the original position of the Adula unit is at the former distal European margin, facing the Valais Ocean, which opened in the Late Jurassic and closed during the Late Cretaceous–Eocene convergence between Europe and Africa–Adria (Dewey et al., 1989). The Briançonnais horst was underthrusted below the Adria margin, following the subduction of the Alpine Tethys. The attempted subduction of the European margin occurred after the closure of the Valais ocean and the collision between Europe and Adria.

At the base the Adula unit is in contact with the Simano Unit. If the contact is not occurring along the Mesozoic metasedimentary cover of the Simano unit, then it is not always well distinguishable, due to the similarity between the Simano basement gneiss, and the overprinting caused by the Barrovian late Cenozoic metamorphism.

At the top, the Adula unit is separated from the Middle Penninic units by the Misox zone (Mesolcina zone of Cavargna-Sani et al., 2014), a thin unit of mainly Valaisan (North Penninic) provenance (e.g., Schmid et al., 1996) composed by several slices of metasedimentary clastic rocks (the "North Penninic Bündnerschiefer," Pleuger et al., 2003), MORB-derived amphibolites and slices of continental basement.

The Adula unit is primarily composed of orthogneiss and paragneiss. The magmatic protoliths of the orthogneiss have Ordovician or Early Permian intrusion ages (Cavargna-Sani et al., 2014; Steck et al., 2013). The paragneisses are frequently interleaved with amphibolites and metacarbonates. Amphibolites often contain eclogitic relicts and well-preserved eclogite boudins are documented in several localities (Brouwer et al., 2005 with references). Slices of the metamorphosed Adula Mesosozic sedimentary cover are mainly preserved in the norther part of the unit (Cavargna-Sani et al., 2014; Galster et al., 2012).

During the Eocene-Oligocene Alpine orogenic cycle, the Adula unit, along with the crustal fragments which now form the Southern Steep Belt, was subducted to mantle depths (Becker, 1993; Evans & Trommsdorff, 1978; Gebauer, 1996; Heinrich, 1986). Metamorphic conditions at peak pressure decrease northward, from 2.5 to 3.0 GPa and ca. 750°C in the south to 2.2 GPa and 750°C in the middle to 1.7 GPa and 640°C in the north (Brouwer et al., 2005; Dale & Holland, 2003). Rocks of the Adula unit experienced HP metamorphism also during the Variscan orogeny. Eclogitic relicts dated to 330–370 Ma are preserved in the northern part of the unit (Liati et al., 2009), whereas eclogites of the southern Adula have 35–47 Ma (Becker, 1993; Brouwer et al., 2005; Liati et al., 2009; Sandmann et al., 2014). In the middle part of the unit both Late Carboniferous (Variscan) and Eocene (Alpine) ages occur (Trescolmen eclogites, Herwartz et al., 2011).

3. The San Bernardino Shear Zone

The SBSZ is up to ca. 500 m-thick, top-to-the-E extensional shear zone atop the Adula unit (Figures 2a and 2b) developed in orthogneiss and paragneiss containing eclogite boudins. Eclogite boudins (Figure 2c) are hosted in

Figure 1. (a) Simplified geological map of the European Alps (after Handy et al., 2010; Schmid et al., 2004), in which the Lepontine Dome has been highlighted together with the extensional structures at its eastern and western borders. (b) Tectonic map of the Lepontine nappe stack (after Herwartz et al., 2011; Pleuger et al., 2008) with reported isotherms for the post nappe-stacking Barrovian metamorphic event crosscutting nappe boundaries (from Todd & Engi, 1997). Rectangle shows the position of the map reported in Figure 2. Eclogite or garnet bearing peridotite localities have been shown with green (Adula Unit) or violet (Cima-Lunga Unit) stars. Boxes illustrate a compilation of peak PT and high-pressure ages (Herwartz et al., 2011; Liati et al., 2009). CL Cima Lunga Unit, L-L Lucomagno-Leventina Unit. Va, Vals; Cf, Confin; VL, Val Large; Tr, Trescolmen; Cv, Calvaresc; Ga, Gagnone; Ar, Alpe Arami; Go, Gorduno; Ca, Caurit; Du, Duria). (c) and (d) Simplified cross sections (after Ring & Glodny, 2021). (c) N-S (A-A′) perpendicular to the regional Alpine strike showing the sequence of crystalline units (Adula, Tambo and Suretta) and interlayered sediment zones, and their structural relationship to the Bergell intrusion. (d) WNW-ESE cross section B-B′.

10.1029/2025TC009045

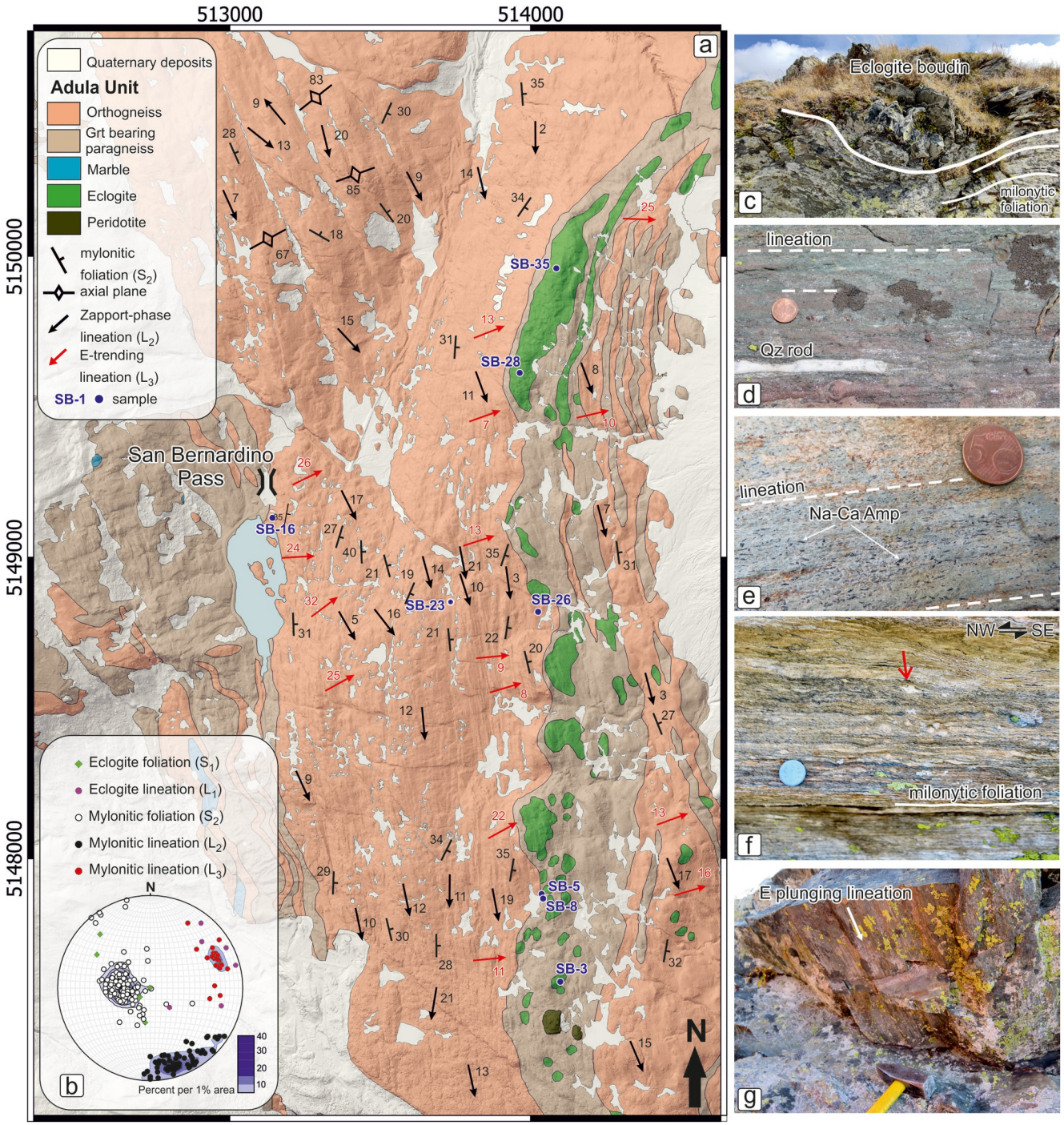

Figure 2. (a) Geological map of the San Bernardino Pass area, WGS84 UTM 32N. (b) Equal area, lower hemisphere stereographic projections of foliation (S_1) and lineation (L_1) in eclogite boudins and, mylonitic foliation (S_2) and lineation referred to the Zapport phase (L_2) and to the orogen parallel extension phase (L_3). (c) Eclogite boudin hosted in paragneiss. (d) Eclogite lineation on foliation plane highlighted by Qz rods and (e) by Na-Ca amphibole. (f) Top-to-the-NW shearing, related to the Zapport-phase (i.e., nappe stacking), in the mylonitic orthogneiss. The red arrow points to a σ-clast. Foliation fish and SC fabric are also evident as kinematic indicators. (g) ENE-plunging lineation becoming predominant close to the Adula/Misox zone boundary.

paragneiss levels that occur close to the Adula-Misox boundary. Boudins range from a few meters to several hundreds of meters in size (Figure 2). They almost invariably display a foliation (S_1 in Figure 2b) and a lineation (L_1) marked by the Shape Preferred Orientation (SPO) of white mica, clinopyroxene and quartz rods (Figures 2d and 2e). Up to 3 mm in size prismatic porphyroblasts of blue amphibole occur in several outcrops. Amphiboles are

weakly to strongly iso-oriented with the eclogitic lineation (Figure 2e), suggesting they crystallized during the late stages of the eclogitic D_1 deformation event. Eclogitic boudins are flattened along the S_2 mylonitic foliation developed in orthogneiss and paragneiss. The eclogitic L_1 lineation appears to be randomly oriented, suggesting a relative rotation with respect to the dominant L_2 mylonitic lineation developed in the host rock (Figure 2b).

The post-eclogitic fabric, namely mylonitic foliation (S_2), is developed mainly in the orthogneiss, whereas no younger fabric than S_1 and L_1 have been observed in the eclogites. The S_2 foliationdips to the E (Figure 2) with an NW–SE trending L_2 lineation (Figure 2b) mainly developed within orthogneisses. The D_2 *L-S* fabric, pervasive all over the investigated area, is associated to a top-to-NW sense of shear ("Zapport phase" of Pleuger et al., 2003), defined on the base of kinematic indicators developed both at the meso (σ and δ clasts, SCC' structures) and at the microscale.

From the San Bernardino Pass area looking toward the E the NE-dipping foliation of the Adula unit is clearly observable, together with the Misox and Tambo units above.

The D_2 mylonitic fabric is overprinted by a younger mylonitic lineation (L_3) developed along the S_2 foliation planes, but oriented at high angle (Figures 2a and 2b) with respect to L_2. L_3 is associated to a top-to-the-E sense of shear, mainly defined from microstructural observations on oriented thin sections (see Section 5), as kinematic indicators at the mesoscale appear to be poorly developed and do not allow to estimate the kinematic vorticity (i.e., simple vs. pure shear component). The ENE to WSW-trending L_3 becomes increasingly pronounced from the bottom (W) to the top (E) of the shear zone itself. L_3 is chiefly developed within orthogneiss or at the rims of the eclogitic boudins (Figure 2f), likely as a consequence of the rheological contrast between eclogite and the host paragneiss. For samples location see Table S1 (available at https://doi.org/10.17632/hctf2rgcnk.1).

4. Analytical Methods

The details of the analytical procedures (i.e., EMPA, $^{40}Ar/^{39}Ar$ dating, thermodynamic modeling, etc.) are described in the following section. Mineral name abbreviations are explained in the caption of Figure 3.

4.1. Electron Probe Micro Analysis

Mineral compositions were measured with the JEOL 8200 Super Probe EMP at the Department of Earth Sciences Ardito Desio, University of Milano. The analysis was carried out using five wavelength dispersive spectrometers with an accelerating voltage of 15 kV, a beam current of 5 nA with a spot size of 3 μm on micas and 1 μm on other minerals. Natural silicates and oxides were used as standards. Analyses were recalculated to atom per formula unit (a.p.f.u.) as follows: white mica analyses were elaborated based on 11 oxygens and considering all Fe as Fe^{2+}; garnet was recalculated based on 8 cations and 24 charges; clinopyroxene analyses were recalculated following the procedure by Cawthorn and Collerson (1974) based on 12 oxygens and considering Fe^{3+} as the acmite component; amphiboles analyses were recalculated based on 23 oxygens and 13 cations plus K, Na, Ca. Amphiboles were classified according to Hawthorne et al. (2012). In all tables, the abbreviations are after Whitney and Evans (2010) except for white mica (Wm).

4.2. $^{40}Ar/^{39}Ar$ Dating

The choice of the dating method for the present eclogite samples was dictated by petrological observations. In these rocks both garnet cores and rims are rich of inclusions in mutual disequilibrium, possibly representing multiple metamorphic stages. The extreme difficulty of obtaining garnet rim separates completely free from included relict phases means that Lu-Hf or U-Pb dating of garnet would not necessarily provide robust data. Therefore we focus on $^{40}Ar/^{39}Ar$ ages to date the growth of phengite in eclogites along the main foliation, at or near peak metamorphism (i.e., a minimum age for HP metamorphism), and the following exhumation stages recorded by the host orthogneisses.

The choice of the $^{40}Ar/^{39}Ar$ method for dating eclogite samples is rooted in the broader framework of the isotopic closure. The term "isotopic closure" comprehend the possibility that, beside temperature, other processes can affect the isotopic system (see Villa, 2002; Montemagni & Villa, 2025, for an exhaustive discussion). Numerous studies have demonstrated that diffusion is negligible compared to fluid-mediated recrystallization in resetting isotopic systems (e.g., Bosse & Villa, 2019; De Sigoyer et al., 2000; Villa et al., 2023) and the idea that volume diffusion alone can modify the isotope record is merely an assumption. Fluid-assisted recrystallization operates

10.1029/2025TC009045

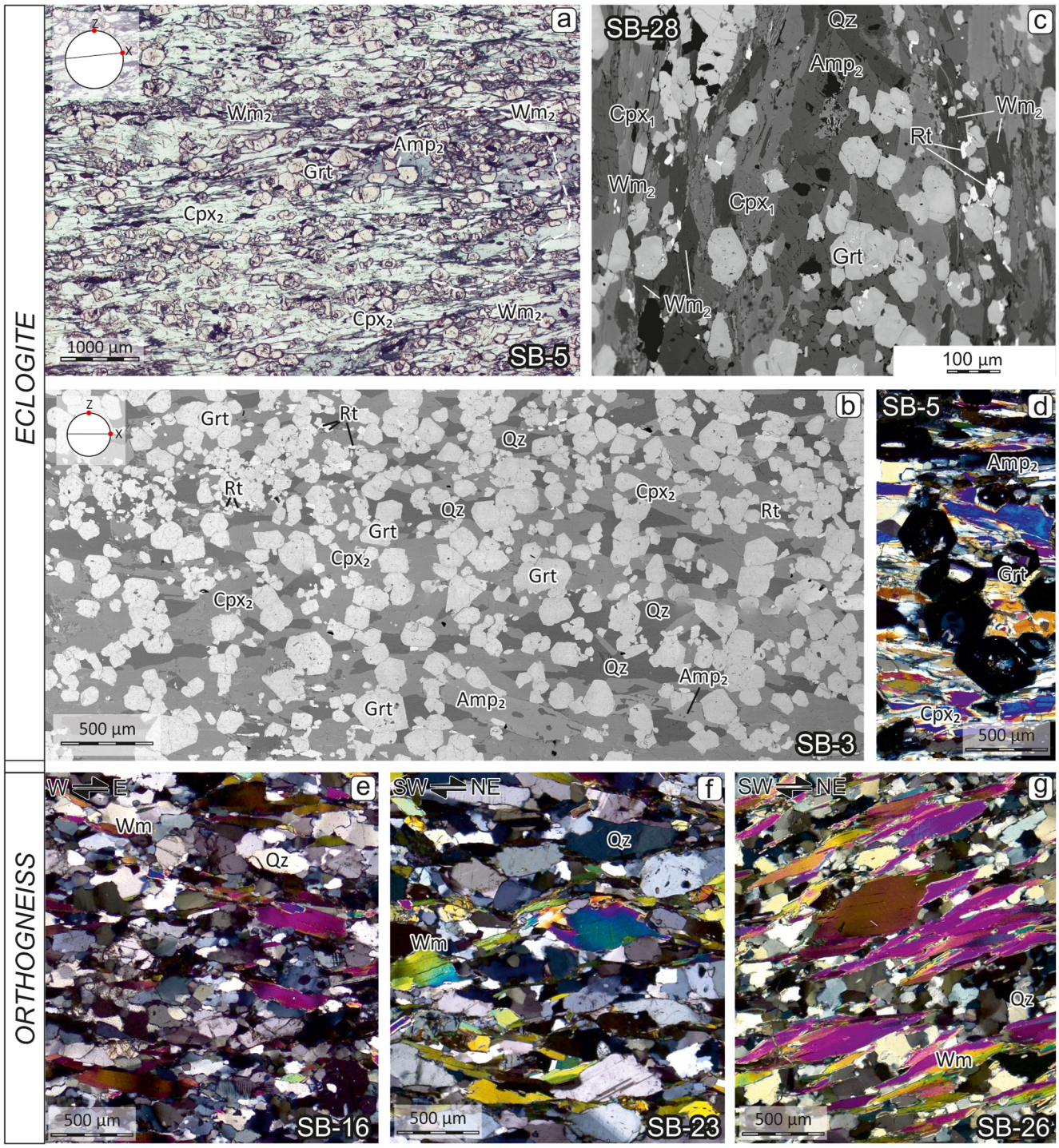

Figure 3. Photomicrographs of San Bernardino eclogites and orthogneisses. (a) Eclogite sample showing the main foliation made of Cpx_1, Amp_2 and Wm_2 surrounding Grt porphyroblasts (parallel polars). (b) BSE panorama of eclogite characterized by a main foliation of Cpx_1, Amp_2 and Wm_2. (c) BSE image of a large Amp2 porphyroblasts syn-kinematic to the eclogitic foliation. Garnet porphyroblasts, when having an aspect ration that differs from 1:1, also appear elongated along the foliation. (d) Cross-polars photo of garnet porphyroblasts within the eclogite, containing inclusions of Wm and Amp. (e), (f) and (g) orthogneiss samples dated by $^{40}Ar/^{39}Ar$ method from bottom to top of the San Bernardino Shear Zone. In (e) the older foliation is still evident, whereas is fully overprinted in (g). The mineral abbreviations are as follows: Amp: amphibole; Ap: apatite; Bt: biotite; Cal: calcite; Chl: chlorite; Cpx: clinopyroxene; Czo: clinozoisite; Dol: dolomite; Grt: garnet; Ilm: ilmenite; Kfs: K-feldspar; Qz: quartz; Pg: paragonite; Pl: plagioclase; Rt: rutile; Ttn: titanite; Wm: white mica; Zr: zircon.

orders of magnitude faster than volume diffusion (Bosse & Villa, 2019); white mica can retain Ar up to temperatures approaching 600°C in the absence of fluids and retrograde reactions (Villa et al., 2014, 2023). This condition has been verified in the eclogitic samples dated in this study through microstructural observations and EMP analyses. Furthermore, thermodynamic modeling and geothermobarometric results indicate that peak temperatures ranged between 525 and 615°C, meaning that all the metamorphic evolution of our samples occurred below, or at most very near, the isotopic closure of phengite.

Dating and resolving discrete *P-T* stages of eclogite-facies rocks was successfully achieved using the $^{40}Ar/^{39}Ar$ technique (e.g., De Sigoyer et al., 2000; Di Vincenzo et al., 2006; Federico et al., 2005), while also showing that excess Ar is negligible (Di Vincenzo et al., 2006; Larson et al., 2023; Villa et al., 2014) in such rocks. It is extremely important not to confuse "excess" Ar with "inherited" Ar to explain unexpected ages (Villa et al., 2014). To assess the possibility of Ar diffusion in our samples, white mica was sieved into the 125–250 μm and 250–500 μm fractions. Identical ages obtained from both size fractions would rule out significant volume diffusion, which is strongly dependent on grain size (Dodson, 1973).

The analytical protocol of choice to date even partly retrograded samples is stepwise heating, as retrograde reactions occur at or below the 5 μm scale (Federico et al., 2005; Villa et al., 2023). The scale of heterogeneities makes any laser-spot analysis (IR, UV, etc.) useless. In contrast, stepwise heating is capable of resolving intergrown phases at any length scale >0.1 μm (Müller et al., 2002).

Samples selected for $^{40}Ar/^{39}Ar$ dating were crushed and sieved in order to separate phengitic white mica from orthogneiss and eclogite for stepwise heating experiments. The separates were enriched in white mica by handpicking under a stereomicroscope. Mineral separates were then cleaned ultrasonically in deionized water and wrapped in aluminum foil. Samples and standards were irradiated for 10 MWh in a fast neutron flux at the McMaster University Research Reactor (Hamilton, CA). Stepwise heating experiments were performed at the Laboratorio di Geocronologia of the University of Milano–Bicocca following the procedure reported in Montemagni and Villa (2021) and Montemagni and Zanchetta (2022). Sample and standards were loaded in a double vacuum resistance furnace attached to a NuInstruments™ Noblesse® noble gas mass spectrometer, equipped with one Faraday collector with a 1,011 Ω resistor and two MasCom™ ion counters. The samples were heated in 8–10 steps for 20 min each. The irradiation intensity factor, *J*, was interpolated for each sample from the gradient defined by the *J* values of the monitors. The ^{40}K decay constant used for the age calculation was 5.543×10^{-4} Ma^{-1} reported in Steiger and Jäger (1977). The vertical flux gradient has been controlled by monitors of McClure Mountain hornblende (MMhb) which were interlayered with the sample disk wraps. The age of the MMhb was assumed as 523.1 Ma (Renne et al., 1998).

4.3. Thermodynamic Modeling and Geothermobarometry

Thermodynamic modeling was performed in the MnO-Na_2O-CaO-K_2O-FeO-MgO-Al_2O_3-SiO_2-H_2O-TiO_2-O (MnNCKFMASTO) system with the software package GeoPS (http://www.geops.org; Xiang & Connolly, 2022), using the revised version (2004, hp04ver.dat) of the thermodynamic database of Holland and Powell (1998) based on an algorithm for the minimization of the Gibbs energy. A carbonate-free eclogite sample was used to derive the chemical composition used for modeling. Sample (SB5, see Table S1, https://doi.org/10.17632/hctf2rgcnk.1 for sample location) was analyzed by Inductively Coupled Plasma Mass Spectrometry for major elements at the ACME analytical laboratories (Vancouver, Canada) after fusion with lithium metaborate/tetraborate and digestion by diluted HNO_3. Loss on ignition was determined by weight difference after ignition at 1,000°C. Blank analyses were always below the minimum detection limit for each element, and the analytical protocol included the analysis of the reference materials (standards) OREAS184, SO-19, OREAS30A and OREAS262 (standards details at https://www.oreas.com). The composition used is the one of sample SB35: SiO_2 (48.46%), Al_2O_3 (17.12%), FeO (12.41%), MgO (6.09%), Na_2O (3.94%), K_2O (1.13%), TiO_2 (2.11%), MnO (0.22%), H_2O (1.2%, based on Loss On Ignition). The equation of state for a binary fluid H_2O-CO_2 of Holland and Powell (1998) was adopted, considering fluid saturated conditions with a pure H_2O fluid.

The used *A-X* solutions are from White and Powell (2002) (WPC), Holland and Powell (2011) (HP11), White et al. (2014) (W), Green et al. (2016) (G): Chl(W) for chlorite, Gt(W) for garnet, Mica(W) for muscovite-paragonite, Crd(W) for cordierite, Bi(W) for biotite, Ctd(W) for chloritoid, St(W) for staurolite, melt(G) for melt, FSP(WPC) for ternary feldspar, Ilm(W) for ilmenite, Opx(W) for orthopyroxene, Omph(G) for omphacite, cAmph(G) for amphibole, EP(H11) for epidote. Pure phases considered in modeling include quartz/coesite, rutile,

titanite, lawsonite and H_2O. The results of forward thermodynamic modeling have been compared with conventional geothermobarometry. The phase equilibrium assemblage of the San Bernardino eclogites (Grt + Cpx + Ph ± Ky) responds to the conditions requested by the geothermometer of Krogh Ravna (2000) and the geothermobarometer of Krogh Ravna and Terry (2004). *P-T* estimates were obtained for three eclogite samples (SB3, SB5a and SB35, see Table S1, https://doi.org/10.17632/hctf2rgcnk.1 for sample details). Cpx–Grt–Ph in textural equilibrium and directly in contact to each other were selected and their composition measured by EPMA analysis.

5. Petrochronology

5.1. Microstructures and Mineral Chemistry

5.1.1. Eclogites

Two types of eclogites crop out within the SBZS: carbonate-free (type 1) and carbonate-bearing (type 2). We focused our attention on type 1 eclogites as they are by far the most abundant and, thanks to their simpler mineralogy, they are more suitable for thermodynamic modeling. Type 1 eclogites mineralogy is made of garnet, clinopyroxene, white mica, amphibole, rutile, quartz, and clinozoisite. Apatite, zircon and ilmenite occur as accessory phases. The mean grain size ranges from <50 μm up to 250 μm for garnet porphyroblasts, 50–350 μm for clinopyroxene and white mica, <100 μm for rutile and up to 2,000 μm for amphiboles porphyroblasts grown on the eclogitic foliation (S_1, Figures 2e and 3).

Garnet porphyroblasts elongated parallel to the eclogitic foliation appear optically zoned, with inclusion-rich cores and clean rims (Figure 3a). Garnet inclusions consist of blue amphibole (Amp_1), white mica (Wm_1), quartz and rare rutile (Rt_1). The pre-eclogitic equilibrium phase assemblage preserved in garnet cores is:

$$Grt_1 + Amp_1 + Wm_1 + Rt_1 + Qz.$$

Garnet rims appear to have grown synkinematically to the S_1 eclogitic foliation, as shown by their slightly elongated idiomorphic habit (Figures 3a and 4). S_1 is marked by the SPO of Cpx_1 and Wm_2. Rutile grains (Rt_2) with an elongated habit (aspect ratio 1:2 to 1:3, Figure 3a) are also parallel to S_1. In some samples also porphyroblasts of clinozoisite (Czo_1) up to 800–1,000 μm occur. The syn-S_1 eclogitic phase assemblage is:

$$Grt_2 + Cpx_1 + Wm_2 + Rt_2 + Qz \pm Czo_1.$$

In a few samples atoll garnet porphyroblasts occur. Radial fractures crosscutting garnet rims and the occurrence of lobate edges, peninsular structures and ameboid relicts at cores suggests that fluid-assisted resorption ad recrystallization occurred (e.g., Faryad et al., 2010). At the core of atoll garnets there are Qz + Cpx + Wm inclusions that display the same composition of minerals along the S_1 eclogitic foliation. Large (up to 2,000 μm, Figures 2e and 3c) blue-colored amphibole porphyroblasts (Amp_2) grow late-to post-kinematic with respect to the S_1 foliation. The HP phase assemblage in eclogites is generally well preserved, with only minor retrogression resulting in symplectites made of Amp_3 + Cpx_2 + Pl + Qz that develop along grain boundaries of Cpx_1 and between Cpx_1 and garnet porphyroblasts.

Type 2 eclogites contain carbonates and paragonitic white mica. Garnet cores of type 2 eclogites have inclusions of Wm_1, Amp_1, Mgs and Qz. White mica (Wm_1) included in garnet cores ha a phengitic composition whereas Wm_2 along foliation is a nearly pure paragonite. The syn-S_1 phase assemblage (Grt_2 + Cpx_2 + Wm_2 + Rt + Qz + Dol) is similar to that of type 1 eclogites, except for the occurrence of dolomite porphyroblasts elongated parallel to S_1. Rare calcite crystals also occur.

Cpx_1 in type 1 eclogite has an omphacitic composition, with $Jd_{50–57}$ and *X*Mg of 0.70–0.80 (Table S2, available at https://doi.org/10.17632/hctf2rgcnk.1). Cpx_2 rarely occurs within symplectites after Cpx_1, together with Amp_3 and Pl. The Na content of Cpx_2 is slightly lower ($Jd_{41–48}$) than in Cpx_1 (Figure 4c).

Garnet porphyroblasts are compositionally zoned, with decreasing Fe, increasing Mg and almost homogeneous Ca contents from core to rim (Figures 4e and 4f). The composition of the inclusion-rich core (Grt_1) is $Alm_{55–62}Pyr_{13–21}Grs_{21–24}Sps_{1–2}$ (Table S3, available at https://doi.org/10.17632/hctf2rgcnk.1). Garnet rims (Grt_2) are mainly inclusion-free and formed around Grt_1 cores varying in thickness from 1/10 to 1/3 of the entire

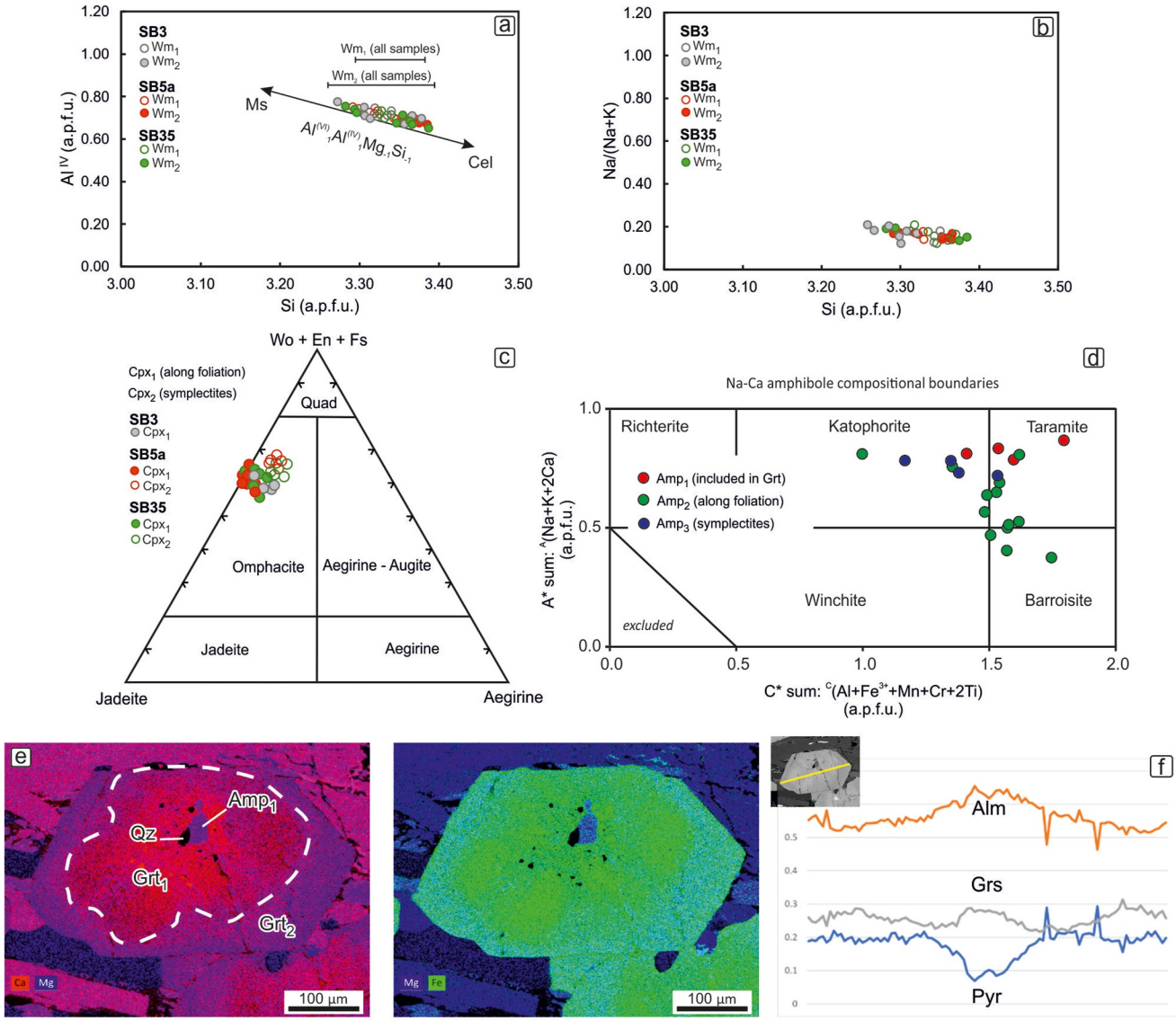

Figure 4. EPMA (Electron Probe Micro Analysis) results showing compositional variation in (a and b) white mica, (c) clinopyroxene, (d) amphibole and (e–g) garnet in eclogite samples.

porphyroblast diameter (Figure 4e). The representative composition of Grt_2 in type 1 eclogites is $Alm_{50–55}Pyr_{20–30}Grs_{18–22}Sps_{0–2}$ (Table S3, https://doi.org/10.17632/hctf2rgcnk.1).

The two white mica generations of type 1 eclogites have phengitic compositions with paragonitic component up to 0.20 Na a.p.f.u.. Wm_1 (included in garnet) and Wm_2 (syn-kinematic along the S_1 eclogitic foliation) display overlapping Si contents, with Wm_1 ranging from 3.30 to 3.38 a.p.f.u. and Wm_2 that displays a wider range of 3.26–3.39 with decreasing Si from core to rim, especially for samples SB3 and SB35 (Figure 4a, Table S4, available at https://doi.org/10.17632/hctf2rgcnk.1).

All amphiboles have composition of the Na-Ca group (Hawthorne et al., 2012). Amp_1 inclusions in garnet cores are Taramite, whereas Amp_2 porphyroblasts that formed late-to post-kinematic with respect to the S_1 eclogitic foliation are display compositions ranging from Taramite to Barroisite (Figure 4d). Amp_1 has a Si content around 6 a.p.f.u. and *X*Mg of 0.4–0.6 (Table S5, available at https://doi.org/10.17632/hctf2rgcnk.1). Amp_2 has both higher Si (ca. 6.5 a.p.f.u.) and *X*Mg (0.65–0.70) with respect to Amp_1 (Table S5, https://doi.org/10.17632/hctf2rgcnk.1). Rare amphiboles grown statically on the eclogitic foliation (Amp_3) have composition in the field of

Katophorite (Figure 4d). The M4 site occupancy by Na is 0.5–0.7 for Amp_1 and 0.9–1.1 for Amp_2 (Table S5, https://doi.org/10.17632/hctf2rgcnk.1).

5.1.2. Orthogneisses

Within the orthogneiss, from bottom to top of the SBSZ (Figures 3e–3g), the S_2, Zapport-phase—the dominant metamorphic event recognized in the Adula unit associated to top-to-N-NW nappe stacking and dated around 36–33 Ma (Pleuger et al., 2003)–related, foliation is gradually overprinted (Figures 3f and 3g) by a younger, sub-parallel, foliation-oriented NNW-SSE and dipping toward the E. This younger foliation is expressed at the microscale by the recrystallization of finer flakes of white mica that envelop older mica fish (Figures 3f and 3g) and become more pronounced toward the top of the SBSZ (Figure 3g). Quartz recrystallization mechanisms are expressed by Grain Boundary Migration (GBM, Passchier & Trouw, 2005) and window and pinning structures in the structurally lowest samples (Figure 3e), and by Bulging (BLG, Passchier & Trouw, 2005) moving structurally upwards (Figures 3f and 3g), coherent with a decreasing temperature during top-to-E driven syn-shearing exhumation.

The composition of white mica marking the mylonitic foliation displays a compositional gradient from the bottom to the top of the shear zone. White micas in samples at the bottom (SB16, see Figure 2) have a higher Si content (3.31–3.43 a.p.f.u.) with respect to mylonitic orthogneisses at the top (3.14–3.19 a.p.f.u.), coherent with progressive recrystallization during exhumation.

5.2. *P-T* Estimates

Conventional geothermobarometric calculations have been performed on type 1 eclogite samples. Due to the absence of kyanite in the peak assemblage, we used a combination of reaction 1 (2gr + py + 3Al-cel = 6d + 3mu) of Krogh Ravna and Terry (2004) with garnet-clinopyroxene Fe^{2+}-Mg geothermometer of Krogh Ravna (2000) as suggested by Krogh Ravna and Terry (2004) for Ky-free eclogites. The complete mineral composition data set has been reported in Figures 4 and 5 and tables (available at https://doi.org/10.17632/hctf2rgcnk.1).

Samples SB-5a and SB-35 of the type 1 eclogites and sample SB-3 of type 2 eclogites were used for calculations. Clinopyroxene (Cpx_1 + phengite (Wm_2) and clinopyroxene-garnet-phengite (Cpx_1 + Grt_2 + Wm_2) triplets were selected for the use of the geothermobarometer. All analyses have been performed on mineral grains in textural equilibrium with the eclogitic mylonitic foliation. The peak *P-T* equilibrium conditions of the eclogites have been determined to be approximately 2.0–2.1 GPa and 520–645°C.

The *P-T* isochemical pseudosection has been obtained with the composition of a carbonate-free eclogite sample SB-35 (See "Methods" for details). Isopleths for Si (a.p.f.u.) in phengite, *X*Ca and *X*Mg in garnet have been calculated for the HP field of the pseudosection (Figure 6). The calculated phase diagram predicts that the Cpx-free equilibrium phase assemblage preserved in garnet cores (Grt_1 + Wm_1 + Amp_1 + Rt_1 + Qz) is stable below 1.0 GPa for temperatures lower than 550°C. Biotite, except for very restricted *P-T* fields, is predicted as a stable phase, but was never observed as inclusion in Grt_1.

The stability field of the eclogitic equilibrium phase assemblage (Grt_2 + Cpx_1 + Wm_2 + Rt_2) is stable at *P* of *c*. 2.4 GPa for $T > 700$°C, whereas, due to the negative slope of the Amp-out reaction, expands to increasing *P* as *T* decreases (Figure 6). Microstructure analysis had shown that blue Na-Ca amphibole (Amp_2), grows subparallel to mylonitic lineation, with a weaker, but still evident SPO, similar in orientation to that of Cpx_1. Amp_2 can thus be considered to have grown during or just after the pressure peak, but still in the *P-T* field of stability of Na-Clinopyroxene. Considering the Si-content of Wm_2 in sample SB35 (Figures 4a and 4b, Table S4, https://doi.org/10.17632/hctf2rgcnk.1) and the Grt_2 composition (Figures 4e and 4f, Table S3, https://doi.org/10.17632/hctf2rgcnk.1), the isopleths related to these minerals define a *P-T* range of 580°–655°C and 2.0–2.35 GPa. *P-T* estimates obtained by conventional geothermobarometry are placed close to the lower *P* limit defined by the calculated isochemical section, with *P* of 2.0–2.2 GPa and *T* of 525°–615°C.

5.3. $^{40}Ar/^{39}Ar$ Geochronology

As isochrons are only meaningful if applied to isochronous and cogenetic minerals, they must not be used on the studied orthogneiss samples. Improperly used isochrons could be misinterpreted to identify inherited Ar (which should never be confused with excess Ar), whereas the accurate identification of heterochemical inclusions

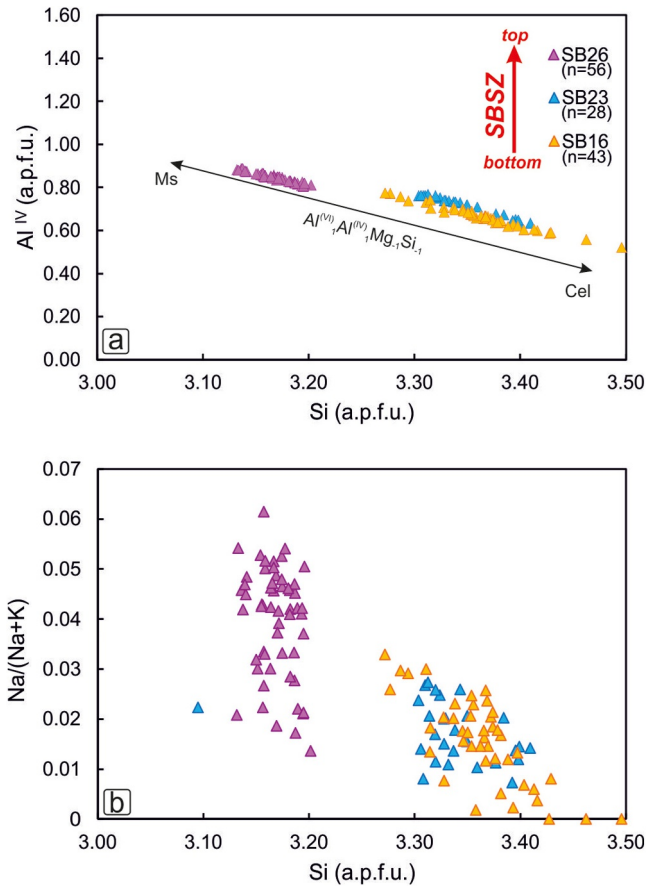

Figure 5. EPMA (Electron Probe Micro Analysis) results showing compositional variation in white mica from orthogneiss samples.

carrying inherited Ar is only provided by the Ca/Cl/K diagrams. For this reason, we refer to the isochemical ages rather than the isochron ages. For the sake of clarity, we report the isochron ages for the eclogite sample for which no evidence of retrogression has been documented.

In two eclogite samples the phengitic white mica (Wm_2) along the mylonitic foliation have been dated. For sample SB5 two distinct mica fractions have been dated (125–250 μm and 250–500 μm, Table S6 available at https://doi.org/10.17632/hctf2rgcnk.1) to check the possible effect of diffusion during retrogression (e.g., Montemagni & Villa, 2021). The two fractions display similar release patterns, with more than 90% ^{39}Ar released in the last four steps (7–10). The obtained ages are 39.70 ± 0.12 Ma for both the 250–500 μm and the 125–250 μm fractions. For sample SB-35 a single fraction has been separated and measured, providing an age of 38.03 ± 0.32 Ma (85.5% of total ^{39}Ar, step 4–9, Figure 7).

The Ar release pattern of phengitic white mica in all orthogneiss samples is quite identical. Three samples collected from the bottom to the top of E shear zone (Figure 2a) have been dated. The Ar spectrum of the structurally lowest sample, SB-16 (Figure 8), consists of steps 4–8 which comprise 81.7% of the total ^{39}Ar and show the lowest Ca/K and Cl/K ratios, resulting in an isochemical age of 36.62 ± 0.08 Ma (see Table S6 for analytical results, available at https://doi.org/10.17632/hctf2rgcnk.1). SB-23 yields an isochemical age of 33.53 ± 0.10 Ma (steps 4–8 release the 77.9% of total ^{39}Ar). The isochemical age of SB-26, the closest to the top of the shear zone, is 29.65 ± 0.06 Ma and it is characterized by a flat portion of the spectrum (steps 5–10) with a 85.9% of ^{39}Ar released and the lowest and homogeneous Ca/K and Cl/K ratios.

6. Discussion

The eclogite bodies of the Adula unit have been studied for a long time since they represent key rocks to understand the pre-Alpine and Alpine subduction-related processes (Figure 9, Liati et al., 2009; Herwartz et al., 2011).

The eclogite bodies of southern Adula are Alpine while in northern Adula they carry pre-Alpine ages (Figure 9b, Liati et al., 2009). Until now, Alpine HP metamorphism had been traced as far north as the Trescolmen locality (Tr in Figure 1b), where Alpine eclogites also preserve HP Variscan relicts (Herwartz et al., 2011). This study provides the first dating of the San Bernardino eclogites, yielding a minimum age of 38–39 Ma. These results extend the documented northern limit of Alpine HP metamorphism within the Adula unit. The consistent peak pressure ages (35–47 Ma; Becker, 1993; Brouwer et al., 2005; Herwartz et al., 2011; Liati et al., 2009; Sandmann et al., 2014) and metamorphic conditions (600–650°C and 2.0–2.5 GPa; Brouwer et al., 2005) suggest that at least the southern half of the Adula unit behave as a coherent crustal block during the Alpine subduction and exhumation.

6.1. Age of Deformation and Structural Evolution of the SBSZ

Atop the Adula unit, in the San Bernardino Pass area, the SBSZ is a *c*. 500 m thick extensional top-to-the-NE shear zone showing an increasing strain gradient toward the east, namely from the bottom to the top of the SBSZ. Only a faint NE to E-trending lineation is observable in the lower portion of the shear zone, where the dominant top-to-the-NW shear fabric prevails. This top-to-the-NW shear fabric is also pervasive in the entire Adula unit (Nagel, 2008) and related to the nappe stacking event during the Zapport phase (36–33 Ma, Pleuger et al., 2003). Only a partial overprint of the top-to-the-NW shearing is visible both at the meso- and microscale, resulting in the growth of a second mica generation (Wm_2), that in turn led to mixed deformation ages, which indicates the maximum age (36 Ma) for the onset of shearing. Approaching the top of the shear zone, the top-to-the-NE related fabric of the SBSZ becomes more pronounced, with Wm_2 that recrystallized along L_3 NE-trending lineation, substituting Wm_1 in orthogneisses (Figure 3). The eastward progressive overprinting of L_3 on L_2

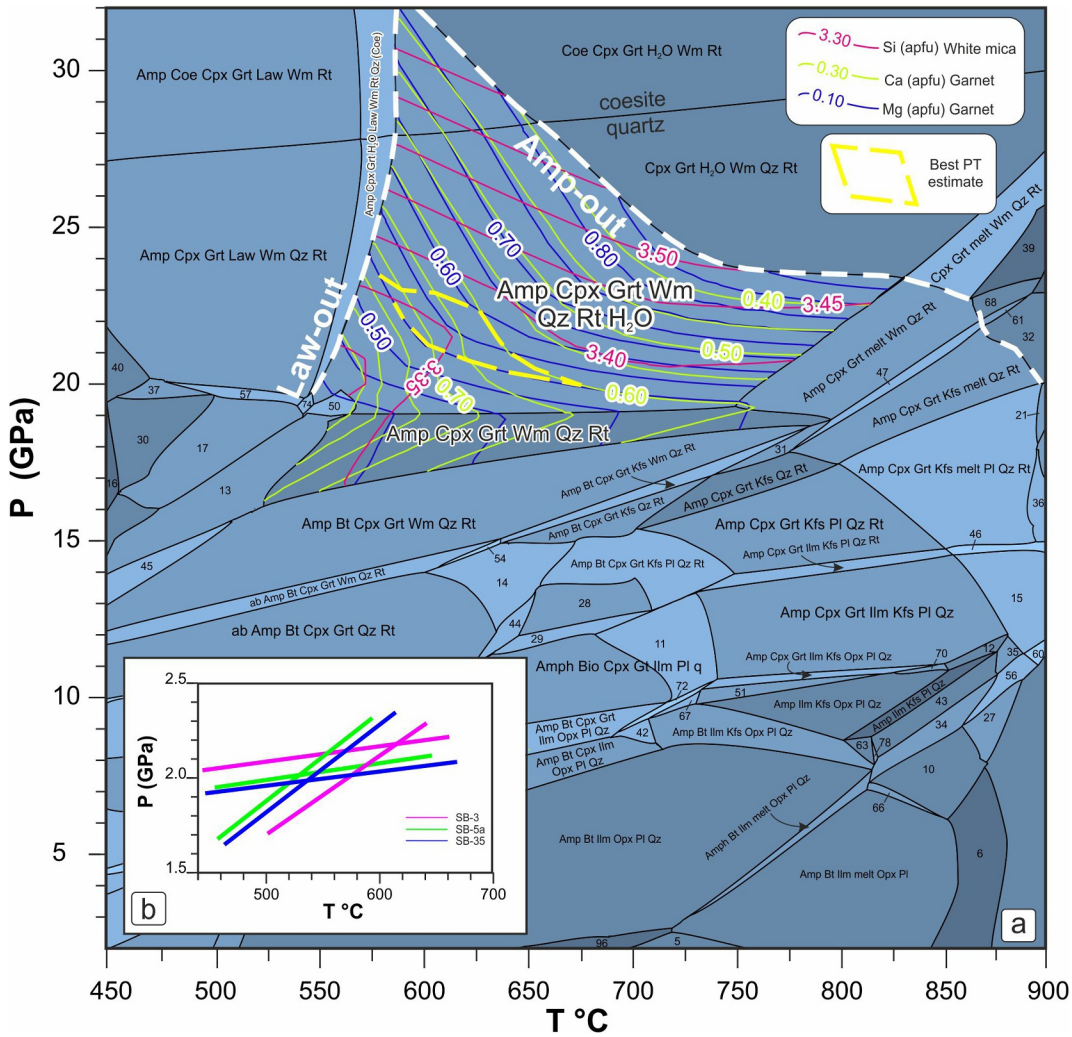

Figure 6. Isochemical phase diagram calculated using the bulk composition of sample SB5. Isopleths for Si in white mica, Ca and Mg in garnet are reported in the stability field of the peak equilibrium phase assemblage. Phase assemblages not reported in full are as follows: (5) Amp, Bt, Ilm, Opx, Pl, H2O; (6) Amp. Ilm, melt, Opx, Pl; (10) Amp, Ilm, Kfs, melt, Opx, Pl; (11) Amp, Bt, Cpx, Grt, Ilm, Kfs, Pl, Qz; (12) Amp, Cpx, Grt, Ilm, Kf, Pl, Qz; (13) Amp, Cpx, Grt, Wm, Qz; (14) ab, Amp, Bt, Cpx, Grt, Kfs, Qz, Rt; (15) Amp, Cpx, Grt, Ilm, Kfs, melt, Pl, Qz; (16) Amp, Cpx, Grt Wm, Rt; (17) Amp, Cpx, Grt, Wm, Qz, Rt, Zo; (18) Amp, Cpx, Grt, melt, Pl, Rt; (21) Amp, Cpx, Grt, Kfs, melt, Pl, Rt; (29) Amp, Bt, Cpx, Ilm, Pl, Rt, Qz; (30) Amp, Cpx, Grt, Wm, Kfs,Q, Rt; (31) Amp, Cpx, Grt, Kfs, Wm, Qz, Rt; (32) Amp, Cpx, Grt, Kfs, melt, Rt; (35) Amp, Cpx, Ilm, Kfs, melt, Pl, Q; (37) Amp, Cpx, Grt, Law, Wm, Rt, Zo; (39) Cpx, Grt, melt Wm, Rt; (40) Amp, Cpx, Grt, Law, Wm, Rt; (42) Amp, Bt, Cpx, Ilm, Kfs, Opx, Pl, Qz; (43) Amp, Ilm, Kfs, melt, Pl, Qz; (45) Amp, Bt, Cpx, Grt, Ms, Q, Rt; (46) Amp, Cpx, Grt, Ilm, Kfs, melt, Pl, Q, Rt; (47) Amp, Cpx, Grt, Kfs, melt, Wm, Q, Rt; (50) Amp, Cpx, Grt, H2O, Wm, Q, Rt; (54) ab, Amp, Bt, Cpx, Grt, Kfs, Wm, Q, Rt; (50) Amp, Cpx, Grt, H2O, Wm, Q, Rt; (54) ab, Amp, Bt, Cpx, Grt, Kfs, Wm, Q, Rt; (56) Amp, Cpx, Ilm, Kfs, melt, Opx, Pl, Q; (57) Amp, Cpx, Grt, Law, Wm, Q, Rt, Zo; (60) Amp, Cpx, Grt, Ilm, Kfs, melt, Opx, Pl, Qz; (61) Amp, Cpx, Grt, Kfs, melt, Wm, Rt; (63) Amp, Bt, Ilm, Kfs, Pl, Qz; (66) Amp, Bt, Grt, Ilm, Kfs, melt, Opx, Pl; (67) Amp, Bt, Grt, Ilm, Kfs, Opx, Pl, Qz; (68) Amp, CPx, Grt, melt, Wm, Rt; (70) Amp, Cpx, Ilm, Kfs, Opx, Pl, Qz; (72) Amp, Bt, Cpx, Grt, Ilm, Kfs, Opx, Pl, Qz; (74) Amp, Cpx, Grt, H2O, Wm, Qz, Rt, Zo; (78) Amp, Bt, Ilm, Kfs, melt, Pl, Qz; (96) Amp, Bt, Ilm, Pl (b) PT estimates calculated with the Krogh Ravna (2000) and the Krogh Ravna and Terry (2004) geothermobarometers for the equilibrium phase assemblage $Wm_2 + Cpx_1 + Grt_2$.

coincides with the younging trend of mica ages: the youngest age (29 Ma, Figure 7) can be considered the maximum age for the onset of top-to-the-E extensional shearing along the SBSZ.

We argue that the crustal extension accommodated by the SBSZ is responsible for part of the exhumation of the eastern flank of the Lepontine Dome, the Ticino culmination (Figures 1a and 9a). Top-to-the-E shearing was not confined to the Middle Penninic nappes or the contact between the Upper Penninic and Austroalpine units

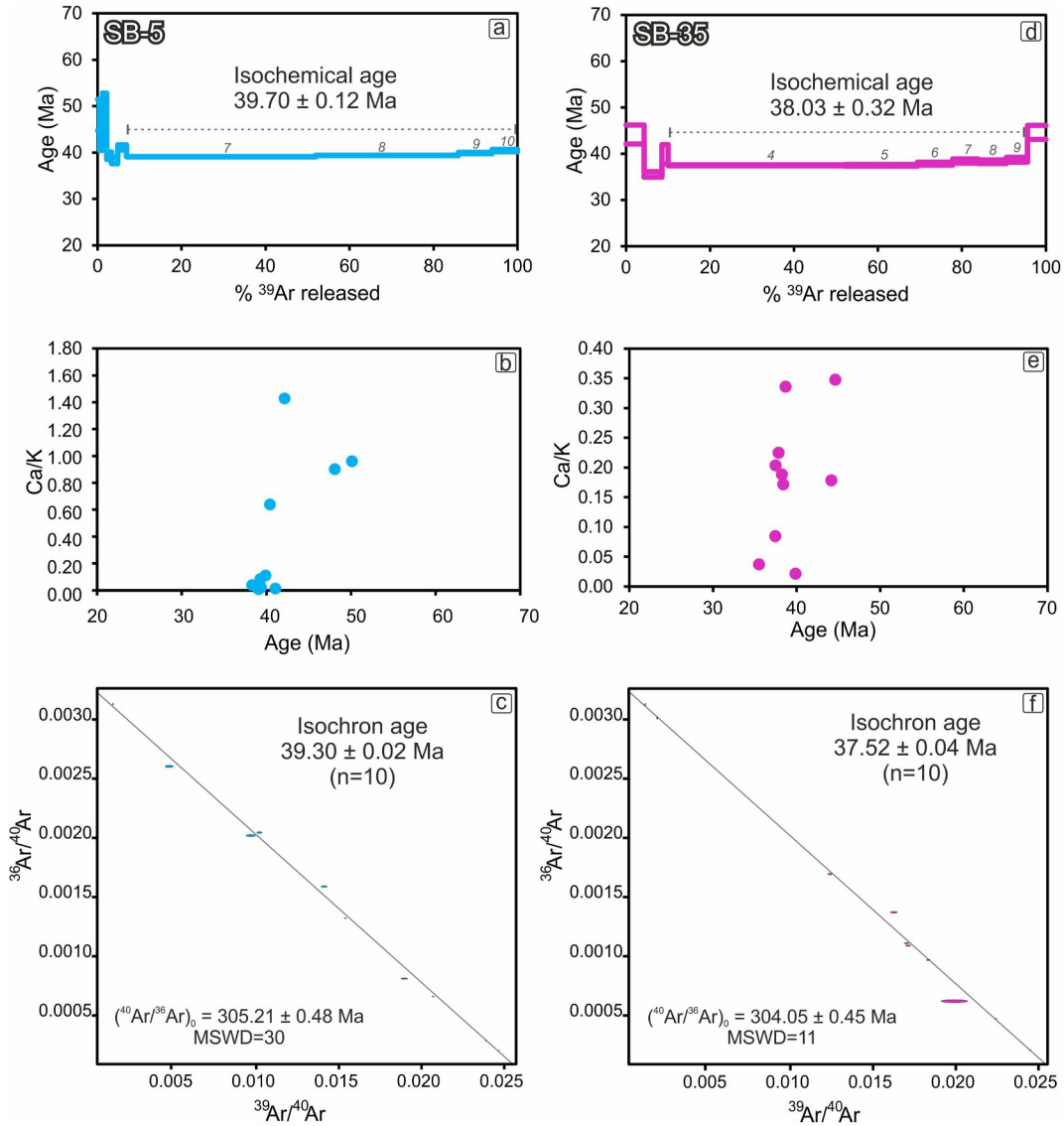

Figure 7. $^{40}Ar/^{39}Ar$ age spectra (mean weighted, isochemical age), Ca/K versus age diagrams and $^{36}Ar/^{40}Ar$ versus $^{39}Ar/^{40}Ar$ for eclogite SB-5 (a, b, and c) and SB-35 (d, e, and f). The isochemical mean weighted age, isochron age, MSWD and $^{40}Ar/^{36}Ar$ intercept have been reported for each sample. All uncertainties are 1σ error.

(e.g., Avers-Turba Mylonite Zone and Martegnas Shear Zone reported in Berger et al., 2005; Frey & Ferreiro Mählmann, 1999; Nagel, 2008; Rosenberg et al., 2021; Ring & Glodny, 2021; Todd & Engi, 1997), but also affected the Adula unit. Our results support the hypothesis proposed by Ring and Glodny (2021), which suggests that the top-to-the-SE ductile extensional shearing was progressively activated from east to west and from top to bottom in the nappe pile. This shearing initially occurred in the Upper Penninic mylonite zones (the Avers-Turba and Martegnas mylonite zones, Ring & Glodny, 2021), before migrating to the Middle Penninic Splügen and Misox zones (Figure 1b), where it reached the top of the Adula unit.

Top-to-the-SE ductile shearing began around 45 Ma, while the Lower Penninic units had yet to reach peak-pressure conditions. The waning stage of this shearing in the Upper and Middle Penninic units persisted until 34 Ma (Price et al., 2018; Ring & Glodny, 2021), just before the peak temperature of the amphibolite facies metamorphism in the Lepontine Dome at 33–31 Ma (e.g., Tagliaferri et al., 2023). Younger ages associated with top-to-the-E extensional shearing (35–31 Ma, Ring & Glodny, 2021) occur in the Splügen and Misox Zone,

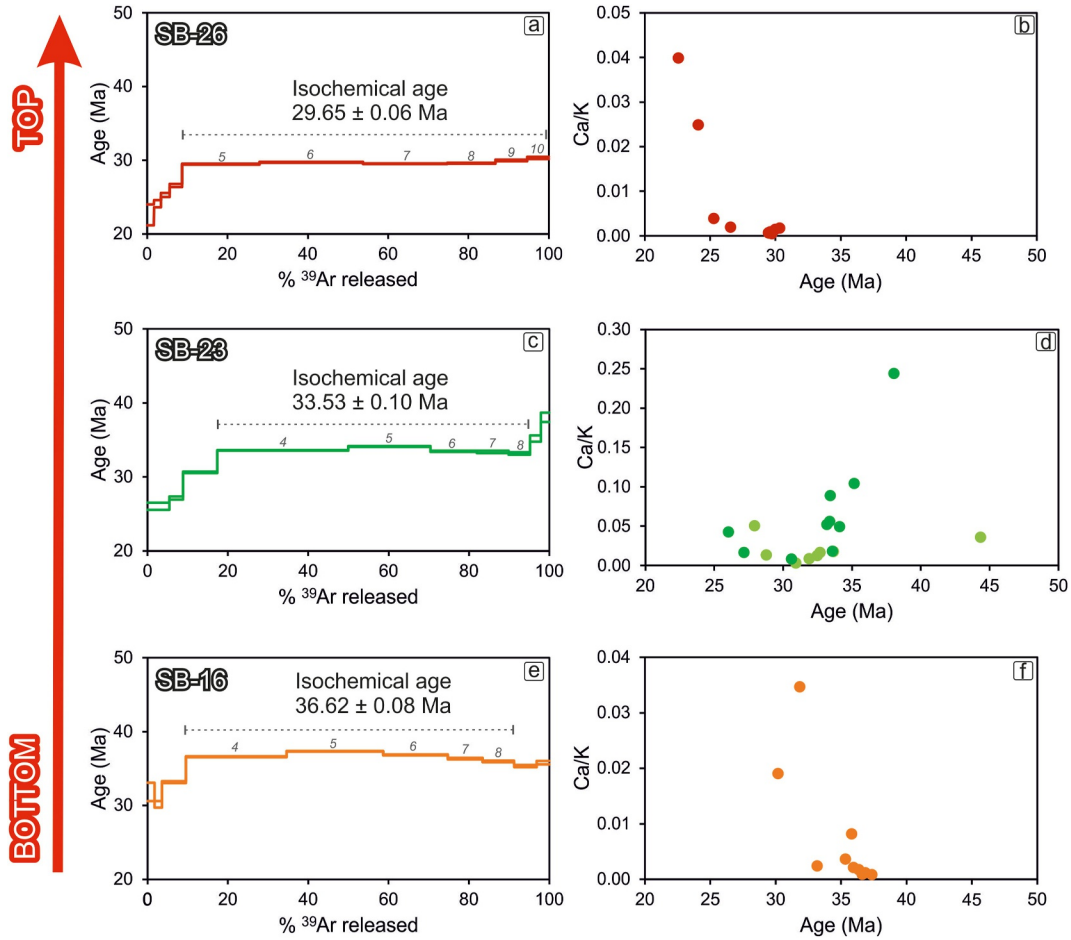

Figure 8. $^{40}Ar/^{39}Ar$ age spectra with obtained mean weighted age and Ca/K versus age diagrams for orthogneiss SB-26 (a, b), SB-23 (c, d) and SB-16 (e, f). The dated fraction size has been reported for each sample. All uncertainties are 1σ error.

corresponding to an intra-Middle Penninic shear zone and to the contact between the Middle and the Lower Penninic nappe stack, respectively.

The 39–38 Ma minimum age of the San Bernardino eclogites confirms that the Adula unit reached HP conditions while top-to-the-SE ductile shearing was active in the upper levels of the growing orogenic wedge. The onset of top-to-the-NW nappe stacking is broadly coeval with the deactivation of the top-to-the-SE extensional shearing in the Upper Penninic structures and its westward migration, slightly rotating to a top-to-the-E direction (Ring & Glodny, 2021).

The top-to-the-NW nappe-stacking of the Lower Penninic units in the Lepontine Dome occurred in the 36–34 Ma time interval (e.g., Nagel, 2008; Steck et al., 2019), and it was largely coeval with amphibolite facies regional metamorphism, leading to widespread crustal anatexis in the Southern Steep Belt (Figures 1a and 1b) and local migmatization along the main tectonic contacts in the southern and central part of the dome (Tagliaferri et al., 2023). Crustal shortening and thrusting of the Lower Penninic HP units above the non-HP units occurred at the same time with orogen-parallel extension, which reduced overburden in the growing Lepontine nappe-stack. As the HP units were exhumed, top-to-the-E shearing progressively migrated downward, affecting the Splügen Zone, the base of the Suretta unit and the Misox Zone before finally activating the SBSZ at ca. 29 Ma, based on our data. The new age of the top-to-the-E mylonites at the top of the Adula unit point to a distributed top-to-the-E shearing reaching the exhuming HP units of the Lepontine Dome by the middle to late Oligocene.

Considering the 29 Ma age of sample SB26 as a mixed age, younger than the other samples, it constrains the onset of SBSZ activity to be no older than 29 Ma. However, given the identical orthogneiss protolith and compositional

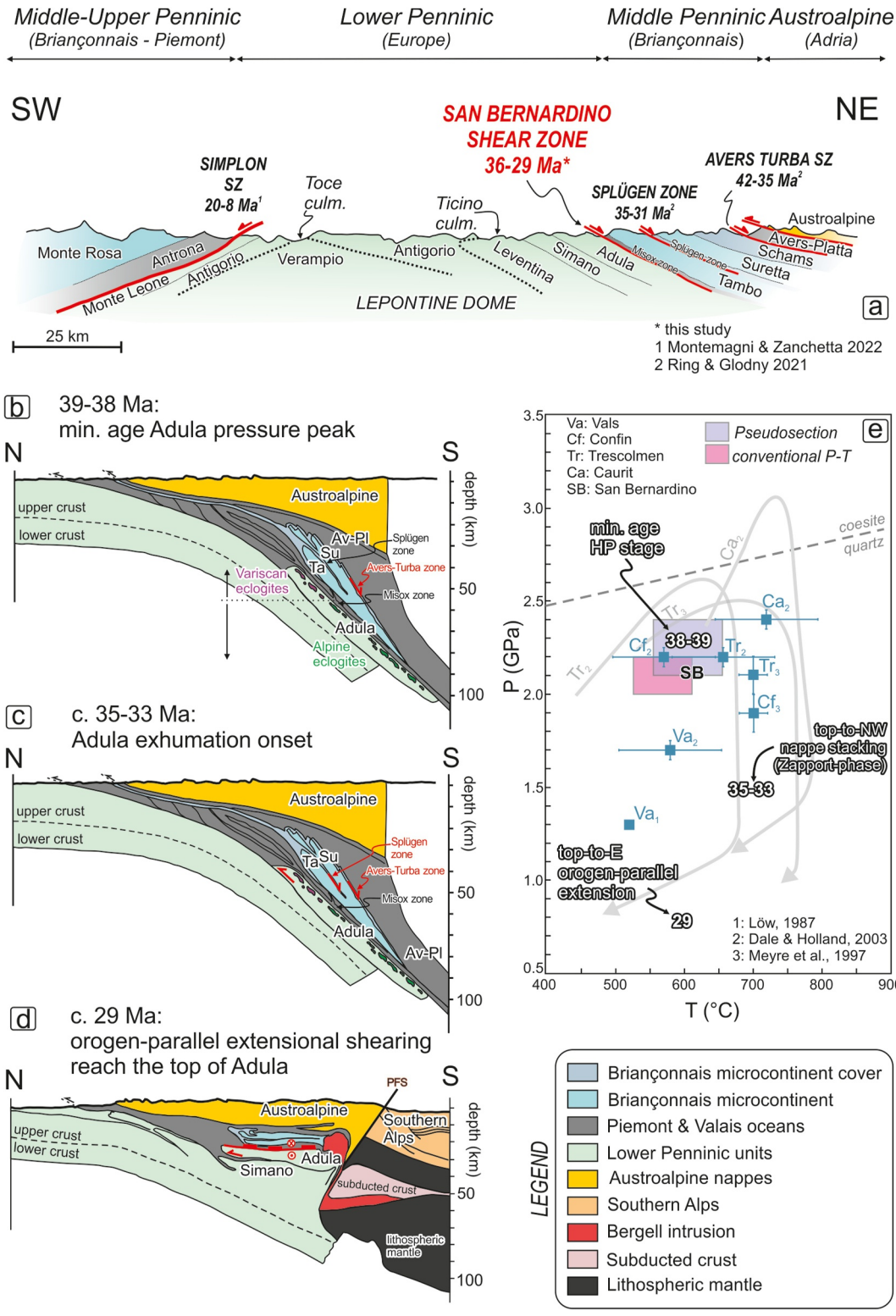

Figure 9.

variations in the micas (Figure 5), the 29 Ma age most likely records the onset of shearing. Accordingly, the structurally lower portion of the SBSZ yields ages comparable to the Zapport phase, while the structurally higher portion reflects the timing of the top-to-the-E extensional shearing event, suggesting a progressive transition from early deformation at depth to later, more localized extensional shearing during exhumation.

6.2. Tectonic Implications

The role of orogen-parallel extension during Adula unit exhumation remains debated. Classical models (e.g., Rosenberg et al., 2021; Schmid et al., 1996) suggest minor or negligible extension, whereas others (Marquer et al., 1996; Pleuger et al., 2003; Ring & Glodny, 2021) argue for a penetrative, long-lasting orogen-parallel extension.

Contrary, in the western flank of the Lepontine Dome, the exhumation of the Toce culmination was fostered by the younger Simplon Fault (Figures 1a and 9a) in the 20–8 Ma time span (Montemagni & Zanchetta, 2022, with references). Some Authors (Meyre et al., 1998; Schlunegger & Willett, 1999), based on similar amount of syn-orogenic extension and age of shearing, proposed that the Forcola Fault (21–18 Ma), the southeastward continuation of the Misox Zone (Figure 1), represents the eastern equivalent of the Simplon Fault. However, the offset of the metamorphic isograds across the Simplon Fault point to a vertical displacement of about 15 km (Grasemann & Mancktelow, 1993), whereas no comparable offset is observed across the Forcola Fault (Ciancaleoni & Marquer, 2008; Frey & Ferreiro Mählmann, 1999) suggesting that the exhumation of the Lepontine Dome is mainly accommodated by localized normal shearing in the west, and by more local tilting, doming and normal shearing and faulting along several structures and nappe-separating metasediments zones (i.e., Misox Zone and Splügen Zone) within Penninic and Austroalpine nappe stack in the east (Rahn, 2005).

Over a short time span (<5 Myrs), the Adula unit experienced HP metamorphism during south dipping continental subduction, developing eclogites at 2–2.5 GPa around 40 Ma in the central-northern portion of the slab (Figures 9b and 9e), followed by a rapid top-to-the-NW directed exhumation (Figure 9c) during the nappe-stacking phase (33–36 Ma, Wiederkher et al., 2008, 2009). Top-to-the-E ductile shearing occurred in the hanging wall of the Misox Zone since at least 45 Ma, testifying for the contemporaneity of orogen-perpendicular shortening and orogen-parallel extension, the last promoting the exhumation of the Adula itself in the 36–29 Ma time span (Figure 9d).

A similar tectonic framework is observed in the Eastern Alps, where the exhumation of the Tauern Window was accommodated by the Brenner Shear Zone in the west and the Katschberg Shear Zone in the east, which exhibited top-to-the-W and top-to-the-E extensional ductile shearing, respectively, since about 25 Ma (e.g., Ratschbacher et al., 1991; Steck, 1984). Hence, as the Tauern Window in the Eastern Alps, the Lepontine Dome in the Central Alps, experienced syn to post-collisional orogen-parallel extensional shearing, facilitating the exhumation of the (U)HP units currently exposed in the Penninic nappe-stack of the Central Alps.

Nevertheless, the extent, duration, and role of orogen-parallel extension in the evolution of convergent plate margins remain debated (Beltrando et al., 2010; Rosenberg & Garcia, 2011). Tectonic switching between orogen-perpendicular lithospheric thickening and orogen-parallel lithospheric thinning has been invoked to explain the evolution of the Oligocene Central Alps (Beltrando et al., 2010). Crustal scale extension within a developing orogenic wedge may emerge as a transient yet dominant deformation style across the entire orogen, driven by episodic lithospheric thinning due to geodynamic changes such as slab rollback, change in convergence velocity and relative motion between the hinge of the subducting slab and the leading edge of the upper plate. Orogen-parallel deformation during ongoing convergence has been documented in other orogens, including the

Figure 9. (a) Structural cross-section through the Lepontine dome (modified from Steck et al., 2013) with shear zones at the western and eastern flank of the dome highlighted. (b)–(d) Tectonic interpretation (after Ring & Glodny, 2021). (b) The Adula reached the pressure peak conditions at a minimum age of 39–38 Ma. The Avers-Turba mylonite zone was active. Eclogites are indicated: violet for Variscan eclogites and green for Alpine eclogites. (c) Beginning of overthrusting during the coherent exhumation of the Adula unit onto the underlying units. In this stage the Splügen zone is also active. (d) At (c) 29 Ma the orogen-parallel extensional shearing reached the top of the Adula unit, partially coeval with thrusting at the bottom of the unit itself. (e) *P-T* estimates and *P-T* paths for various localities in the Adula unit. Violet and pink squares indicates the *P-T* estimates obtained in this study, via pseudosection and conventional *P-T* respectively. The ages for high-pressure metamorphism, exhumation and orogen-parallel extension have been reported (Löw, 1987).

Himalayas (e.g., Coleman, 1996; Jessup et al., 2008) and the Spanish Variscan Belt (e.g., Balda et al., 1995), suggesting that syn-convergent, orogen-parallel extensional shear zones represent a mechanism for accommodating crustal exhumation in collisional settings. In the Annapurna-Manaslu region of the Himalayan belt, the Chame detachment (Coleman, 1996; Searle & Godin, 2003), accommodated oblique, top-to-the-west–directed during early Miocene peak metamorphism at the upper structural levels of the Greater Himalayan Sequence and remained active during retrograde metamorphism. West-trending stretching lineations associated with west-directed movement on the Chame Detachment overprint earlier north-trending ones, indicating that the west-oriented fabrics developed through west-directed shearing rather than reorientation of a pre-existing north-verging structure. West-directed, orogen-parallel extension along the Chame Detachment in the Annapurna-Manaslu region was broadly coeval with north-directed, orogen-perpendicular displacement along the South Tibetan Detachment System approximately 15 km to the east (e.g., Coleman, 1996).

Traditionally, the structural evolution of the Alps has been interpreted through orogenic wedge models, where nappes formed at crustal depths via ductile underthrusting at the base of the wedge (e.g., Handy et al., 2010; Platt, 1986; Polino et al., 1990). However, the discovery of (U)HP rocks recording pressures far exceeding the pressures predicted by orogenic wedge models (see Jolivet et al., 2003 with references), has led to alternative hypotheses to explain the structural evolution of Central Alps. These hypotheses include buoyancy-driven exhumation, which can occur through three main mechanisms: (a) continuous return flow of rocks within a subduction channel, (b) upward flow of individual buoyant rock units through denser material, and (c) lithospheric extension and associated upward flow due to slab rollback (Schenker et al., 2015 with references). Our data support the hypothesis that the final exhumation stage of the Adula unit was driven by top-to-the-E extensional shearing, which distinctly began before 30 Ma, broadly coeval with the emplacement of the Bergell pluton at ca. 20 km depth between 32 and 28 Ma (e.g., Blanckenburg, 1992). As the Lepontine Dome was tectonically exhumed, top-to-the-E shearing progressively migrated to deeper structural levels, reaching the top of the Adula unit at ca. 30 Ma.

The evolution of the SBSZ must be considered within the broader dynamics of the Alpine orogenic wedge. During convergence the minimum conditions of HP peak (~2.0–2.4 GPa, 580°–655°C at 38–39 Ma) were rapidly followed by top-to-the-NW nappe stacking, reflecting critical taper conditions in a compressive wedge. However, as burial peaked and crustal thickening progressed, the system transitioned into a gravitationally unstable configuration, prompting a switch to orogen-parallel extension. The activation of top-to-the-E extensional shear zones such as the SBSZ illustrates this shift in kinematics captured in the progressive overprinting of early fabrics and the partial to complete resetting of $^{40}Ar/^{39}Ar$ mica ages to 29 Ma. We found no direct evidence of the process or combination of processes that drove this transition. However, several mechanisms that have already been proposedto promote rapid eclogite exhumation and a change in tectonic transport direction may have been active at the Eocene-Oligocence boundary in the Central Alps: arrival at the subduction trench of continental blocks and/or non stationary trench can lead to transient behaviors in subduction regimes, promoting buoyancy-driven exhumation (Brun & Faccenna, 2008; Husson et al., 2009) or exhumation favored by local divergence and slab roll back in an overall convergent setting (Malusà et al., 2015). The occurrence of magmatic activity associated with crustal partial melting in the Central Alps from ca. 32 Ma (Blackenburg, 1992; Tagliaferri et al., 2023) progressively modified crustal rheology with a thermal induced weaking that interested the present-day southern sector of the Lepontine Dome (e.g., Burri et al., 2005). Such dynamic orogenic feedbacks promoted a switch from crustal accretion to ductile thinning and exhumation. The contemporaneity of amphibolite-facies metamorphism and extensional fabrics supports a model in which intrusion of Bergell pluton (32–28 Ma) and extension were coeval yet partitioned, reflecting a complex interplay between deep burial, magma emplacement, lateral extrusion, and surface uplift in an evolving orogenic wedge, suggesting a link between the mode of deformation and the strength of the deforming wedge.

7. Conclusions

This study presents new constraints on the tectonometamorphic evolution of the Adula unit in the eastern Central Alps, focusing on the San Bernardino Pass area. Through integrated structural, petrological, thermodynamic modeling, and $^{40}Ar/^{39}Ar$ geochronological analyses, we document the first occurrence of Alpine HP metamorphism in the northern sector of the Adula unit. $^{40}Ar/^{39}Ar$ dating of synkinematic phengitic white mica yields consistent minimum ages of 38–39 Ma, coinciding with peak metamorphic conditions of 2.0–2.35 GPa and 580°–655°C.

The extensional SBSZ, a top-to-the-E ductile shear zone, is developed within the upper Adula unit and accommodated part of the unit exhumation. Progressive textural overprinting of top-to-the-NW nappe-stacking fabrics (Zapport phase) by top-to-the-E mylonitic fabrics related to the SBSZ, is matched by a progressive $^{40}Ar/^{39}Ar$ age resetting with L_3 lineation associated to the synkinematic growth of a second white mica generation in orthogneisses, marking the transition from crustal shortening to extensional shearing.

The combination of petrochronological and structural data highlights a rapid tectonic evolution from subduction (~39 Ma), through nappe stacking (36–34 Ma), to final exhumation along extensional shear zone (~30 Ma), within a timeframe of less than 10 Myrs.

This transition reflects a major shift in orogenic dynamics, from compressive crustal thickening under critical taper conditions to gravitational collapse and orogen-parallel extension.

Although a direct connection with deeper crustal processes cannot be demonstrated due to the lack of direct evidence, the onset of extensional shearing in the SBSZ could be tentatively associated with slab rollback and lower crustal flow, that, together with thermal weakening from partial melting, created a dynamically unstable orogenic wedge. Notably, the contemporaneity of amphibolite-facies metamorphism and the emplacement of the Bergell pluton (~32–28 Ma) with top-to-the-E shearing suggests partitioned, yet genetically linked processes of exhumation and magmatism.

These results support a model in which the eastern Lepontine Dome was exhumed via distributed orogen-parallel extension along several shear zones activating from upper structural levels downwards, reaching the top of the Adula unit at ~30 Ma.

The consistent P-T conditions and timing across the unit of the HP metamorphism suggest that the Adula unit behaved as a coherent crustal block during Alpine subduction and exhumation.

Conflict of Interest

The authors declare no conflicts of interest relevant to this study.

Data Availability Statement

EMPA and $^{40}Ar/^{39}Ar$ data are available in the Bicocca Open Archive Research Data free-access repository (https://doi.org/10.17632/hctf2rgcnk.1). Pseusosection was created through software package GeoPS (Xiang & Connolly, 2022) available at http://www.geops.org. Details for reference materials (OREAS, SO) used for major elements analysis are available at https://www.oreas.com. $^{40}Ar/^{39}Ar$ data reduction procedures, corrected for mass spectrometer background, ion counter gains, blank measurements, source fractionation and decay of ^{37}Ar since irradiation, were processed in the in-house CalcolAr Excel spreadsheet, in which also all the associated uncertainties are propagated. EMP analyses were normalized and recalculated with an in-house excel spreadsheet.

Acknowledgments
C. Montemagni, N. Malaspina and S. Zanchetta acknowledge the support of Project MUR—Dipartimento di Eccellenza 2023–2027 "TECLA" (Grant 2023-NAZ-0212). We thank A. Risplendente for the EMPA sessions performed at the Unitech COSPECT (University of Milano, Italy). We warmly thank Editor Djordje Grujic and the Associate Editor for editorial handling and useful comments. We also thank Jaroslaw Majka and three anonymous reviewers for their constructive reviews, which significantly improved the first version of this manuscript. Open access publishing facilitated by Universita degli Studi di Firenze, as part of the Wiley - CRUI-CARE agreement.

References

Balda, M. D., Catalán, J. M., & Arribas, P. A. (1995). Syn-collisional extensional collapse parallel to the orogenic trend in a domain of steep tectonics: The Salamanca detachment zone (central Iberian zone, Spain). *Journal of Structural Geology*, *17*(2), 163–182. https://doi.org/10.1016/0191-8141(94)e0042-w

Becker, H. (1993). Garnet peridotite and eclogite Sm-Nd mineral ages from the lepontine dome (Swiss Alps): New evidence for Eocene high-pressure metamorphism in the central Alps. *Geology*, *21*(7), 599–602. https://doi.org/10.1130/0091-7613(1993)021<0599:GPAESN>2.3.CO;2

Beltrando, M., Lister, G. S., Rosenbaum, G., Richards, S., & Forster, M. A. (2010). Recognizing episodic lithospheric thinning along a convergent plate margin: The example of the early Oligocene Alps. *Earth Science Review*, *103*(3–4), 81–98. https://doi.org/10.1016/j.earscirev.2010.09.001

Berger, A., Mercolli, I., & Engi, M. (2005). The central Lepontine Alps: Notes accompanying the tectonic and petrographic map sheet Sopra Ceneri (1:100,000). *Schweizerische Mineralogische und Petrographische Mitteilungen*, *85*, 109–146.

Beyssac, O., Negro, F., Simoes, M., Chan, Y. C., & Chen, Y. G. (2008). High-pressure metamorphism in Taiwan: From oceanic subduction to arc-continent collision? *Terra Nova*, *20*(2), 118–125. https://doi.org/10.1111/j.1365-3121.2008.00796.x

Bosse, V., & Villa, I. M. (2019). Petrochronology and hygrochronology of tectono-metamorphic events. *Gondwana Research*, *71*, 76–90. https://doi.org/10.1016/j.gr.2018.12.014

Brouwer, F. M., Burri, T., Engi, M., & Berger, A. (2005). Eclogite relics in the Central Alps: PT-evolution, Lu-Hf ages and implications for formation of tectonic mélange zones. *Schweizerische Mineralogische und Petrographische Mitteilungen*, *85*, 147–174.

Brun, J. P., & Faccenna, C. (2008). Exhumation of high-pressure rocks driven by slab rollback. *Earth and Planetary Science Letters*, *272*(1–2), 1–7. https://doi.org/10.1016/j.epsl.2008.02.038

Burri, T., Berger, A., & Engi, M. (2005). Tertiary migmatites in the Central Alps: Regional distribution, field relations, conditions of formation, and tectonic implications. *Schweizerische Mineralogische und Petrographische Mitteilungen*, *85*, 215–232.

Cavargna-Sani, M., Epard, J. L., & Steck, A. (2014). Structure, geometry and kinematics of the northern Adula nappe (Central Alps). *Swiss Journal of Geosciences*, *107*(2–3), 135–156. https://doi.org/10.1007/s00015-014-0175-7

Cawthorn, R. G., & Collerson, K. D. (1974). The recalculation of pyroxene endmember parameters and the estimation of ferrous and ferric iron content from electron microprobe analyses. *American Mineralogist*, *59*(11–12), 1203–1208.

Chemenda, A. I., Mattauer, M., Malavieille, J., & Bokun, A. N. (1995). A mechanism for syn-collisional rock exhumation and associated normal faulting: Results from physical modelling. *Earth and Planetary Science Letters*, *132*(1–4), 225–232. https://doi.org/10.1016/0012-821x(95)00042-b

Ciancaleoni, L., & Marquer, D. (2008). Late Oligocene to early Miocene lateral extrusion at the eastern border of the Lepontine Dome of the Central Alps (Bergell and Insubric areas, eastern Central Alps). *Tectonics*, *27*(4), TC4008. https://doi.org/10.1029/2007TC002196

Coleman, M. E. (1996). Orogen-parallel and orogen-perpendicular extension in the central Nepalese Himalayas. *Geological Society of America Bulletin*, *108*(12), 1594–1607. https://doi.org/10.1130/0016-7606(1996)108<1594:opaope>2.3.co;2

Dale, J., & Holland, T. J. B. (2003). Geothermobarometry, P–T paths and metamorphic field gradients of high-pressure rocks from the Adula Nappe, Central Alps. *Journal of Metamorphic Geology*, *21*(8), 813–829. https://doi.org/10.1046/j.1525-1314.2003.00483.x

de Sigoyer, J., Chavagnac, V., Blichert-Toft, J., Villa, I. M., Luais, B., Guillot, S., et al. (2000). Dating the Indian continental subduction and collisional thickening in the northwest Himalaya: Multichronology of the Tso Morari eclogites. *Geology*, *28*(6), 487–490. https://doi.org/10.1130/0091-7613(2000)28<487:DTICSA>2.0.CO;2

Dewey, J. F., Helman, M. L., Knott, S. D., Turco, E., & Hutton, D. H. W. (1989). Kinematics of the western mediterranean. *Geological Society of London Special Publications*, *45*(45), 265–283. https://doi.org/10.1144/GSL.SP.1989.045.01.15

Di Vincenzo, G., Tonarini, S., Lombardo, B., Castelli, D., & Ottolini, L. (2006). Comparison of ^{40}Ar–^{39}Ar and Rb–Sr data on phengites from the UHP Brossasco–Isasca Unit (Dora Maira Massif, Italy): Implications for dating white mica. *Journal of Petrology*, *47*(7), 1439–1465. https://doi.org/10.1093/petrology/egl018

Dodson, M. H. (1973). Closure temperature in cooling geochronological and petrological systems. *Contributions to Mineralogy and Petrology*, *40*(3), 259–274. https://doi.org/10.1007/bf00373790

Engi, M., Berger, A., & Roselle, G. T. (2001). Role of the tectonic accretion channel in collisional orogeny. *Geology*, *29*(12), 1143–1146. https://doi.org/10.1130/0091-7613(2001)029<1143:rottac>2.0.co;2

Evans, B. W., & Trommsdorff, V. (1978). Petrogenesis of garnet lherzolite, Cima di Gagnone, Lepontine Alps. *Earth and Planetary Science Letters*, *40*(3), 333–348. https://doi.org/10.1016/0012-821x(78)90158-9

Faryad, S., Klápová, H., & Nosál, L. (2010). Mechanism of formation of atoll garnet during high-pressure metamorphism. *Mineralogical Magazine*, *74*(1), 111–126. https://doi.org/10.1180/minmag.2010.074.1.111

Federico, L., Capponi, G., Crispini, L., Scambelluri, M., & Villa, I. M. (2005). ^{39}Ar/^{40}Ar dating of high-pressure rocks from the Ligurian Alps: Evidence for a continuous subduction–exhumation cycle. *Earth and Planetary Science Letters*, *240*(3–4), 668–680. https://doi.org/10.1016/j.epsl.2005.09.062

Federico, L., Crispini, L., Scambelluri, M., & Capponi, G. (2007). Ophiolite mélange zone records exhumation in a fossil subduction channel. *Geology*, *35*(6), 499–502. https://doi.org/10.1130/g23190a.1

Frey, M., & Ferreiro Mählmann, R. (1999). Alpine metamorphism of the Central Alps. *Schweizerische Mineralogische und Petrographische Mitteilungen*, *79*(1), 135–154.

Galster, F., Cavargna-Sani, M., Epard, J. L., & Masson, H. (2012). New stratigraphic data from the Lower Penninic between the Adula nappe and the Gotthard massif and consequences for the tectonics and the paleogeography of the central Alps. *Tectonophysics*, *579*, 37–55. https://doi.org/10.1016/j.tecto.2012.05.029

Gebauer, D. (1996). A P-T-t path for an (ultra) high-pressure ulramafic/mafic rock-association and its felsic country-rocks based on SHRIMP-dating of magmatic and metamorphic zircon domains. Example: Alpe Arami (Central Swiss Alps). In *Earth processes reading the isotopic Code, geophysical monograph* (Vol. 95, pp. 307–329). American Geophysical Union. https://doi.org/10.1029/gm095p0307

Gerya, T. V., Stöckhert, B., & Perchuk, A. L. (2002). Exhumation of high-pressure metamorphic rocks in a subduction channel: A numerical simulation. *Tectonics*, *21*, TC1056. https://doi.org/10.1029/2002TC001406

Grasemann, B., & Mancktelow, N. S. (1993). Two-dimensional thermal modelling of normal faulting: The Simplon Fault zone, central alps, Switzerland. *Tectonophysics*, *225*(3), 155–165. https://doi.org/10.1016/0040-1951(93)90277-Q

Green, E. C. R., White, R. W., Diener, J. F. A., Powell, R., Holland, T. J. B., & Palin, R. M. (2016). Activity–composition relations for the calculation of partial melting equilibria in metabasic rocks. *Journal of Metamorphic Geology*, *34*(9), 845–869. https://doi.org/10.1111/jmg.12211

Grujic, D., Warren, C. J., & Wooden, J. L. (2011). Rapid synconvergent exhumation of Miocene-aged lower orogenic crust in the eastern Himalaya. *Lithosphere*, *3*(5), 346–366. https://doi.org/10.1130/l154.1

Hacker, B. R., & Gerya, T. V. (2013). Paradigms, new and old, for ultrahigh-pressure tectonism. *Tectonophysics*, *603*, 79–88. https://doi.org/10.1016/j.tecto.2013.05.026

Handy, M. R., Schmid, S. M., Bousquet, R., Kissling, E., & Bernoulli, D. (2010). Reconciling plate-tectonic reconstructions of Alpine Tethys with the geological–geophysical record of spreading and subduction in the Alps. *Earth-Science Reviews*, *102*(3–4), 121–158. https://doi.org/10.1016/j.earscirev.2010.06.002

Hawthorne, F. C., Oberti, R., Harlow, G. E., Maresch, W. V., Martin, R. F., Schumacher, J. C., & Welch, M. D. (2012). Nomenclature of the amphibole supergroup. *American Mineralogist*, *97*(11–12), 2031–2048. https://doi.org/10.2138/am.2012.4276

Heinrich, C. A. (1986). Eclogite facies regional metamorphism of hydrous mafic rocks in the Central Alpine Adula Nappe. *Journal of Petrology*, *27*(1), 123–154. https://doi.org/10.1093/petrology/27.1.123

Herwartz, D., Nagel, T. J., Münker, C., Scherer, E. E., & Froitzheim, N. (2011). Tracing two orogenic cycles in one eclogite sample by Lu-Hf garnet chronometry. *Nature Geoscience*, *4*(3), 178–183. https://doi.org/10.1038/ngeo1060

Holland, T. J. B., & Powell, R. (1998). An internally consistent thermodynamic data set for phases of petrological interest. (version 4) [Dataset]. *Journal of Metamorphic Geology*, *16*(3), 309–343. https://doi.org/10.1111/j.1525-1314.1998.00140.x

Holland, T. J. B., & Powell, R. (2011). An improved and extended internally consistent thermodynamic dataset for phases of petrological interest, involving a new equation of state for solids. *Journal of Metamorphic Geology*, *29*(3), 333–383. https://doi.org/10.1111/j.1525-1314.2010.00923.x

Husson, L., Brun, J. P., Yamato, P., & Faccenna, C. (2009). Episodic slab rollback fosters exhumation of HP—UHP rocks. *Geophysical Journal International*, *179*(3), 1292–1300. https://doi.org/10.1111/j.1365-246x.2009.04372.x

Jessup, M. J., Newell, D. L., Cottle, J. M., Berger, A. L., & Spotila, J. A. (2008). Orogen-parallel extension and exhumation enhanced by denudation in the Trans-Himalayan Arun River gorge, Ama Drime Massif, Tibet-Nepal. *Geology*, *36*(7), 587–590. https://doi.org/10.1130/G24722A.1

Jolivet, L., Faccenna, C., Goffe, B., Burov, E., & Agard, P. (2003). Subduction tectonics and exhumation of high-pressure metamorphic rocks in the Mediterranean orogens. *American Journal of Science*, *303*(5), 353–409. https://doi.org/10.2475/ajs.303.5.353

Kossak-Glowczewski, J., Froitzheim, N., Nagel, T. J., Pleuger, J., Keppler, R., Leiss, B., & Régent, V. (2017). Along-strike shear-sense reversal in the Vals-Scaradra Shear Zone at the front of the Adula Nappe (Central Alps, Switzerland). *Swiss Journal of Geosciences*, *110*(2), 677–697. https://doi.org/10.1007/s00015-017-0270-7

Krogh Ravna, E. J. (2000). The garnet–clinopyroxene Fe2þ–Mg geothermometer: An updated calibration. *Journal of Metamorphic Geology*, *18*(2), 211–219. https://doi.org/10.1046/j.1525-1314.2000.00247.x

Krogh Ravna, E. J., & Terry, M. P. (2004). Geothermobarometry of UHP and HP eclogites and schists - An evaluation of equilibria among garnetclinopyroxene-kyanite-phengite- coesite/quartz. *Journal of Metamorphic Geology*, *22*(6), 579–592. https://doi.org/10.1111/j.1525-1314.2004.00534.x

Larson, K. P., Button, M., Shrestha, S., & Camacho, A. (2023). A comparison of $^{87}Rb/^{87}Sr$ and $^{40}Ar/^{39}Ar$ dates: Evaluating the problem of excess ^{40}Ar in Himalayan mica. *Earth and Planetary Science Letters*, *609*, 118058. https://doi.org/10.1016/j.epsl.2023.118058

Liati, A., Gebauer, D., & Fanning, C. M. (2009). Geochronological evolution of HP metamorphic rocks of the Adula nappe, Central Alps, in pre-Alpine and Alpine subduction cycles. *Journal of the Geological Society*, *166*(4), 797–810. https://doi.org/10.1144/0016-76492008-033

Löw, S. (1987). Die tektono-metamorphe Entwicklung der nördlichen Adula-Decke. Beiträge zur Geologischen Karte der Schweiz.

Malusà, M. G., Faccenna, C., Baldwin, S. L., Fitzgerald, P. G., Rossetti, F., Balestrieri, M. L., et al. (2015). Contrasting styles of (U) HP rock exhumation along the Cenozoic Adria-Europe plate boundary (Western Alps, Calabria, Corsica). *Geochemistry, Geophysics, Geosystems*, *16*(6), 1786–1824. https://doi.org/10.1002/2015GC005767

Mancktelow, N. S. (1985). The Simplon Line: A major displacement zone in the western Lepontine Alps. *Eclogae Geologicae Helvetiae*, *78*, 73–96.

Marquer, D., Challandes, N., & Baudin, T. (1996). Shear zone patterns and strain distribution at the scale of a Penninic nappe: The Suretta nappe (Eastern Swiss Alps). *Journal of Structural Geology*, *18*(6), 753–764. https://doi.org/10.1016/s0191-8141(96)80009-5

Merle, O., & Guillier, B. (1989). The building of the Swiss Central Alps: An experimental approach. *Tectonophysics*, *165*(1–4), 41–56. https://doi.org/10.1016/0040-1951(89)90034-6

Meyre, C., Marquer, D., Schmid, S. M., & Ciancaleoni, L. (1998). Syn-orogenic extension along the Forcola fault: Correlation of alpine deformations in the Tambo and Adula nappes (eastern Penninic Alps). *Eclogae Geologicae Helvetiae*, *91*(3), 409–420.

Montemagni, C., & Villa, I. M. (2021). Geochronology of Himalayan shear zones: Unravelling the timing of thrusting from structurally complex fault rocks. *Journal of the Geological Society*, *178*(6), 1–13. https://doi.org/10.1144/jgs2020-235

Montemagni, C., & Villa, I. M. (2025). Dating deformation by the $^{40}Ar/^{39}Ar$ method: A review. *Italian Journal of Geosciences*, *144*(2), 250–263. https://doi.org/10.3301/IJG.2025.06

Montemagni, C., & Zanchetta, S. (2022). Constraining kinematic and temporal evolution of a normal-sense shear zone: Insights into the Simplon Shear Zone (Western Alps). *Journal of Structural Geology*, *156*, 104557. https://doi.org/10.1016/j.jsg.2022.104557

Müller, W., Kelley, S. P., & Villa, I. M. (2002). Dating fault-generated pseudotachylytes: Comparison of $^{40}Ar/^{39}Ar$ stepwise-heating, laser-ablation and Rb/Sr microsampling analyses. *Contribution to Mineralogy and Petrology*, *144*, 57–77. https://doi.org/10.1007/s00410-002-0381-6

Nagel, T. J. (2008). Tertiary subduction, collision and exhumation recorded in the Adula nappe, central Alps. *Geological Society of London Special Publications*, *298*(1), 365–392. https://doi.org/10.1144/sp298.17

Nagel, T. J., De Capitani, C., & Frey, M. (2002). Isograds and P-T evolution in the eastern Lepontine Alps (Graubünden, Switzerland). *Journal of Metamorphic Geology*, *20*(3), 309–324. https://doi.org/10.1046/j.1525-1314.2002.00368.x

Passchier, C. W., & Trouw, R. A. J. (2005). *Microtectonics*. Springer Verlag.

Piccoli, F., Lanari, P., Hermann, J., & Pettke, T. (2022). Deep subduction, melting, and fast cooling of metapelites from the Cima Lunga Unit, Central Alps. *Journal of Metamorphic Geology*, *40*(1), 121–143. https://doi.org/10.1111/jmg.12621

Platt, J. P. (1986). Dynamics of orogenic wedges and the uplift of high-pressure metamorphic rocks. *Geological Society of America Bulletin*, *97*(9), 1037–1053. https://doi.org/10.1130/0016-7606(1986)97<1037:doowat>2.0.co;2

Pleuger, J., Hundenborn, R., Kremer, K., Babinka, S., Kurz, W., Jansen, E., & Froitzheim, N. (2003). Structural evolution of Adula nappe, Misox zone, and tambo nappe in the San Bernardino area: Constraints for the exhumation of the Adula eclogites. *Österreichischen Geologischen Gesellschaft*, *94*, 99–122.

Pleuger, J., Nagel, T. J., Walter, J. M., Jansen, E., & Froitzheim, N. (2008). On the role and importance of orogen-parallel and -perpendicular extension, transcurrent shearing, and backthrusting in the Monte Rosa nappe and the Southern Steep Belt of the Alps (Penninic zone, Switzerland and Italy). *Geological Society of London Special Publications*, *298*(1), 251–280. https://doi.org/10.1144/sp298.13

Polino, R. (1990). Tectonic erosion at the Adria margin and accretionary processes for the Cretaceous orogeny of the Alps. *Mémoire de la Societe géologique de France*, *156*, 345–367.

Price, J. B., Wernicke, B. P., Cosca, M. A., & Farley, K. A. (2018). Thermochronometry across the Austroalpine-Pennine boundary, Central Alps, Switzerland: Orogen-perpendicular Normal Fault Slip on a Major "Overthrust" and its implications for orogenesis. *Tectonics*, *37*(3), 724–757. https://doi.org/10.1002/2017TC004619

Rahn, M. K. (2005). Apatite fission track ages from the Adula nappe: Late-stage exhumation and relief evolution. *Schweizerische Mineralogische und Petrographische Mitteilungen*, *85*, 233–245.

Ratschbacher, L., Frisch, W., Linzer, H.-G., & Merle, O. (1991). Lateral extrusion in the Eastern Alps; part 2, structural analysis. *Tectonics*, *10*(2), 257–271. https://doi.org/10.1029/90tc02623

Regorda, A., Spalla, M. I., Roda, M., Lardeaux, J. M., & Marotta, A. M. (2021). Metamorphic facies and deformation fabrics diagnostic of subduction: Insights from 2D numerical models. *Geochemistry, Geophysics, Geosystems*, *22*(10), e2021GC009899. https://doi.org/10.1029/2021gc009899

Renne, P. R., Swisher, C. C., Deino, A. L., Karner, D. B., Owens, T. L., & DePaolo, D. J. (1998). Intercalibration of standards, absolute ages and uncertainties in $^{40}Ar/^{39}Ar$ dating. *Chemical Geology*, *145*(1–2), 117–152. https://doi.org/10.1016/s0009-2541(97)00159-9

Ring, U., & Glodny, J. (2021). The importance of tangential motion in the Central Alps: Kinematic analysis and RbSr dating of mylonitic rocks from the Pennine nappes in the eastern Central Alps. *Earth-Science Reviews*, *218*, 103644. https://doi.org/10.1016/j.earscirev.2021.103644

Roda, M., Spalla, M. I., & Marotta, A. M. (2012). Integration of natural data within a numerical model of ablative subduction: A possible interpretation for the Alpine dynamics of the Austroalpine crust. *Journal of Metamorphic Geology*, *30*(9), 973–996. https://doi.org/10.1111/jmg.12000

Rosenberg, C. L., Bellahsen, N., Rabaute, A., & Girault, J. B. (2021). Distribution, style, amount of collisional shortening, and their link to Barrovian metamorphism in the European Alps. *Earth-Science Reviews*, *222*, 103774. https://doi.org/10.1016/j.earscirev.2021.103774

Rosenberg, C. L., & Garcia, S. (2011). Estimating displacement along the Brenner Fault and orogen-parallel extension in the Eastern Alps. *International Journal of Earth Sciences*, *100*(5), 1129–1145. https://doi.org/10.1007/s00531-011-0645-3

Rubatto, D., Regis, D., Hermann, J., Boston, K., Engi, M., Beltrando, M., & McAlpine, S. R. B. (2011). Yo-yo subduction recorded by accessory minerals in the Italian Western Alps. *Nature Geoscience*, *4*(5), 338–342. https://doi.org/10.1038/ngeo1124

Sandmann, S., Nagel, T. J., Herwartz, D., Fonseca, R. O. C., Kurzawski, R. M., Münker, C., & Froitzheim, N. (2014). Lu–Hf garnet systematics of a polymetamorphic basement unit: New evidence for coherent exhumation of the Adula Nappe (Central Alps) from eclogite-facies conditions. *Contributions to Mineralogy and Petrology*, *168*(5), 1075. https://doi.org/10.1007/s00410-014-1075-6

Schenker, F. L., Schmalholz, S. M., Moulas, E., Pleuger, J., Baumgartner, L. P., Podladchikov, Y., et al. (2015). Current challenges for explaining (ultra) high-pressure tectonism in the Pennine domain of the Central and Western Alps. *Journal of Metamorphic Geology*, *33*(8), 869–886. https://doi.org/10.1111/jmg.12143

Schlunegger, F., & Willett, S. (1999). Spatial and temporal variations in exhumation of the central Swiss Alps and implications for exhumation mechanisms. *Geological Society of London Special Publications*, *154*(1), 157–179. https://doi.org/10.1144/GSL.SP.1999.154.01.07

Schmid, S. M., Fügenschuh, B., Kissling, E., & Schuster, R. (2004). Tectonic map and overall architecture of the Alpine orogen. *Eclogae Geologicae Helvetiae*, *97*(1), 93–117. https://doi.org/10.1007/s00015-004-1113-x

Schmid, S. M., Pfiffner, O. A., Froitzheim, N., Schönborn, G., & Kissling, E. (1996). Geophysical-geological transect and tectonic evolution of the Swiss-Italian alps. *Tectonics*, *15*(5), 1036–1064. https://doi.org/10.1029/96tc00433

Searle, M. P., & Godin, L. (2003). The South Tibetan detachment and the Manaslu leucogranite: A structural reinterpretation and restoration of the Annapurna-Manaslu Himalaya, Nepal. *The Journal of Geology*, *111*(5), 505–523. https://doi.org/10.1086/376763

Stampfli, G. M., Mosar, J., Marquer, D., Marchant, R., Baudin, T., & Borel, G. (1998). Subduction and obduction processes in the Swiss Alps. *Tectonophysics*, *296*(1–2), 159–204. https://doi.org/10.1016/s0040-1951(98)00142-5

Steck, A. (1984). Structures et deformations tertiaires dans les Alpes centrales. *Eclogae Geologicae Helvetiae*, *77*, 55–100.

Steck, A., Della Torre, F., Keller, F., Pfeifer, H. R., Hunziker, J., & Masson, H. (2013). Tectonics of the Lepontine Alps: Ductile thrusting and folding in the deepest tectonic levels of the Central Alps. *Swiss Journal of Geosciences*, *106*(3), 427–450. https://doi.org/10.1007/s00015-013-0135-7

Steck, A., Epard, J. L., & Masson, H. (2019). The Maggia nappe: An extruding sheath fold basement nappe in the Lepontine gneiss dome of the Central Alps. *International Journal of Earth Sciences*, *108*(8), 2429–2442. https://doi.org/10.1007/s00531-019-01771-1

Steiger, R., & Jäger, E. (1977). Subcommission on geochronology: Convention on the use of decay constants in geo-and cosmochronology. *Earth and Planetary Science Letters*, *36*(3), 359–362. https://doi.org/10.1016/0012-821x(77)90060-7

Stöckhert, B., & Gerya, T. V. (2005). Pre-collisional high pressure metamorphism and nappe tectonics at active continental margins: A numerical simulation. *Terra Nova*, *17*(2), 102–110.

Tagliaferri, A., Schenker, F. L., Ulianov, A., Maino, M., & Schmalholz, S. M. (2023). Implications of new geological mapping and U-Pb zircon dating for the Barrovian tectono-metamorphic evolution of the Lepontine dome (Central European Alps). *Geochemistry, Geophysics, Geosystems*, *24*(3), e2022GC010772. https://doi.org/10.1029/2022GC010772

Todd, C. S., & Engi, M. (1997). Metamorphic field gradients in the Central Alps. *Journal of Metamorphic Geology*, *15*(4), 513–530. https://doi.org/10.1111/j.1525-1314.1997.00038.x

Trommsdorff, V. (1990). Metamorphism and tectonics in the Central Alps: The Alpine lithospheric mélange of Cima Lunga and Adula. *Memorie della Societa Geologica Italiana*, *45*, 39–49.

Tumiati, S., Zanchetta, S., Pellegrino, L., Ferrario, C., Casartelli, S., & Malaspina, N. (2018). Granulite-facies overprint in garnet peridotites and kyanite eclogites of Monte Duria (Central Alps, Italy): Clues from srilankite- and sapphirine-bearing symplectites. *Journal of Petrology*, *59*(1), 115–152. https://doi.org/10.1093/petrology/egy021

Vannucchi, P., Sage, F., Morgan, J. P., Remitti, F., & Collot, J.-Y. (2012). Toward a dynamic concept of the subduction channel at erosive convergent margins with implications for interplate material transfer. *Geochemistry, Geophysics, Geosystems*, *13*, Q02003. https://doi.org/10.1029/2011GC003846

Villa, I. M. (2002). Isotopic closure. *Terra Nova*, *10*(1), 42–47. https://doi.org/10.1046/j.1365-3121.1998.00156.x

Villa, I. M., Bucher, S., Bousquet, R., Kleinhanns, I. C., & Schmid, S. M. (2014). Dating polygenetic metamorphic assemblages along a transect across the Western Alps. *Journal of Petrology*, *55*(4), 803–830. https://doi.org/10.1093/petrology/egu007

Villa, I. M., Glodny, J., Peillod, A., Skelton, A., & Ring, U. (2023). Petrochronology of polygenetic white micas (Naxos, Greece). *Journal of Metamorphic Geology*, *41*(3), 401–423. https://doi.org/10.1111/jmg.12700

von Blackenburg, F. (1992). Combined high-precision chronometry and geochemical tracing using accessory minerals: Applied to the Central-Alpine Bergell intrusion (central Europe). *Chemical Geology*, *100*(1–2), 19–40. https://doi.org/10.1016/0009-2541(92)90100-j

White, R. W., & Powell, R. (2002). Melt loss and the preservation of granulite facies mineral assemblages. *Journal of Metamorphic Geology*, *20*(7), 621–632. https://doi.org/10.1046/j.1525-1314.2002.00206_20_7.x

White, R. W., Powell, R., Holland, T. J. B., Johnson, T. E., & Green, E. C. R. (2014). New mineral activity-composition relations for thermodynamic calculations in metapelitic systems. *Journal of Metamorphic Geology*, *32*(3), 261–286. https://doi.org/10.1111/jmg.12071

Whitney, D. L., & Evans, B. W. (2010). Abbreviations for names of rock-forming minerals. *American Mineralogist*, *95*(1), 185–187. https://doi.org/10.2138/am.2010.3371

Wiederkehr, M., Bousquet, R., Schmid, S. M., & Berger, A. (2008). From subduction to collision: Thermal overprint of HP/LT meta-sediments in the north-eastern Lepontine Dome (Swiss Alps) and consequances regarding the tectono-metamorphic evolution of the Alpine orogenic wedge. *Swiss Journal of Geosciences*, *101*(1), 127–155. https://doi.org/10.1007/s00015-008-1289-6

Wiederkehr, M., Sudo, M., Bousquet, R., Berger, A., & Schmid, S. M. (2009). Alpine orogenic evolution from subduction to collisional thermal overprint: The $^{40}Ar/^{39}Ar$ age constraints from the Valaisan Ocean, central Alps. *Tectonics*, *28*(6), TC6009. https://doi.org/10.1029/2009TC002496

Wolff, R., Hölzer, K., Hetzel, R., Dunkl, I., & Anczkiewicz, A. A. (2024). Late-orogenic extension ceases with waning plate convergence: The case of the Simplon normal fault (Swiss Alps). *Journal of Structural Geology*, *179*, 105049. https://doi.org/10.1016/j.jsg.2024.105049

Xiang, H., & Connolly, J. A. (2022). GeoPS: An interactive visual computing tool for thermodynamic modelling of phase equilibria [Software]. *Journal of Metamorphic Geology*, *40*(2), 243–255. https://doi.org/10.1111/jmg.12626